MOLECULAR BIOLOGY

Active DNA demethylation of developmental *cis*-regulatory regions predates vertebrate origins

Ksenia Skvortsova[1,2]*, Stephanie Bertrand[3], Danila Voronov[4]†, Paul E. Duckett[1], Samuel E. Ross[1,2,5], Marta Silvia Magri[6], Ignacio Maeso[6], Robert J. Weatheritt[1,7], Jose Luis Gómez Skarmeta[6]‡, Maria Ina Arnone[4], Hector Escriva[3], Ozren Bogdanovic[1,5,6]*

DNA methylation [5-methylcytosine (5mC)] is a repressive gene-regulatory mark required for vertebrate embryogenesis. Genomic 5mC is tightly regulated through the action of DNA methyltransferases, which deposit 5mC, and ten-eleven translocation (TET) enzymes, which participate in its active removal through the formation of 5-hydroxymethylcytosine (5hmC). TET enzymes are essential for mammalian gastrulation and activation of vertebrate developmental enhancers; however, to date, a clear picture of 5hmC function, abundance, and genomic distribution in nonvertebrate lineages is lacking. By using base-resolution 5mC and 5hmC quantification during sea urchin and lancelet embryogenesis, we shed light on the roles of nonvertebrate 5hmC and TET enzymes. We find that these invertebrate deuterostomes use TET enzymes for targeted demethylation of regulatory regions associated with developmental genes and show that the complement of identified 5hmC-regulated genes is conserved to vertebrates. This work demonstrates that active 5mC removal from regulatory regions is a common feature of deuterostome embryogenesis suggestive of an unexpected deep conservation of a major gene-regulatory module.

INTRODUCTION

Metazoan development is governed by the activity of cis-regulatory DNA elements that serve as binding platforms for transcription factors controlling spatial and temporal gene expression (*1*, *2*). In vertebrates, one of the major gene-regulatory mechanisms entails methylation of the fifth carbon of the cytosine pyrimidine ring (5mC) within the DNA (*3*). 5mC is a predominantly repressive gene-regulatory mark, which in vertebrates displays unparalleled developmental dynamics. Mammalian embryogenesis is characterized by two rounds of genome-wide 5mC reprogramming that take place in the preimplantation embryo and in the developing germ line (*4*). Global 5mC erasure occurs through a combination of active and passive 5mC removal mechanisms, such as the exclusion of maintenance DNA methyltransferase (DNMT1) from the nucleus (*5*, *6*), and targeted oxidation of 5mC by ten-eleven translocation (TET) enzymes, respectively (*7*, *8*). TET enzymes oxidize 5mC through a series of reactions involving 5-hydroxymethylcytosine (5hmC), 5-formylcytosine (5fC), and 5-carboxylcytosine (5caC) intermediates, the latter two of which can be excised by base excision repair pathways, thus leading to the restoration of unmethylated cytosine at affected sites (*9*). Apart from participating in mammalian global 5mC erasure, TET enzymes drive targeted 5mC removal from promoters and enhancers required for vertebrate gastrulation (*10*) and organ formation (*11*). TET activity is thus crucial for orchestrating gene-regulatory programs associated with cell fate determination and tissue differentiation. TET depletion accompanied by 5hmC reduction results in enhancer hypermethylation and reduced chromatin accessibility in vertebrate embryos (*11*, *12*), delayed gene induction during cellular differentiation (*13*), and skewed lineage differentiation (*14*, *15*). Loss of 5mC in DNMT mutant cells, on the other hand, was shown to result in the activation of intragenic enhancers (*16*), together highlighting the significance of timely DNA demethylation in the regulation of cis-regulatory elements and lineage specification.

In stark contrast to vertebrates, which are characterized by high genomic 5mC levels (~80%), most nonvertebrate organisms sampled to date have mosaic DNA methylation patterns that vary widely in their content, genomic distribution, and function (*17*). Notable exceptions to that rule include *Drosophila melanogaster* (*18*) and *Caenorhabditis elegans* (*19*), whose genomes are devoid of 5mC, and the demosponge *Amphimedon queenslandica*, the genome of which displays vertebrate-like genomic hypermethylation (*20*). Those exceptions notwithstanding, a common feature of invertebrate 5mC patterning is the association of 5mC with gene bodies of actively transcribed genes (*21*). 5mC has been shown to prevent precocious transcription from cryptic transcription start sites located within gene bodies (*22*, *23*). However, it is currently underexplored whether any other aspects of 5mC-mediated genome regulation are evolutionarily maintained across the invertebrate-vertebrate boundary. For example, TET proteins are present in most nonvertebrate genomes (*24*) where their function has been linked to RNA hydroxymethylation (*25*), production of 5hmC in the germ line (*26*), or regulation of alternative splicing (*27*). Except for a single study that used enzyme-linked immunosorbent assay–based approaches to demonstrate global 5hmC developmental loss in the Pacific Sea gooseberry (*Pleurobrachia bachei*) (*28*), it is not yet clear to what extent nonvertebrate organisms use 5mC and consequently TET proteins and 5hmC for developmental gene regulation. Moreover,

[1]Genomics and Epigenetics Division, Garvan Institute of Medical Research, Sydney, Australia. [2]St. Vincent's Clinical School, Faculty of Medicine, University of New South Wales, Sydney, Australia. [3]Sorbonne Université, CNRS, Biologie Intégrative des Organismes Marins (BIOM), Observatoire Océanologique, Banyuls-sur-Mer, France. [4]Biology and Evolution of Marine Organisms (BEOM), Stazione Zoologica Anton Dohrn, Naples, Italy. [5]School of Biotechnology and Biomolecular Sciences, University of New South Wales, Sydney 22, Australia. [6]Centro Andaluz de Biología del Desarrollo, CSIC-Universidad Pablo de Olavide-Junta de Andalucía, Seville, Spain. [7]EMBL Australia, Garvan Institute of Medical Research, Sydney, Australia.
*Corresponding author. Email: k.skvortsova@garvan.org.au (K.S.); o.bogdanovic@gmail.com (O.B.)
†Present address: Max Planck Institute of Evolutionary Biology, 24306 Plön, Germany.
‡Deceased.

base-resolution hydroxymethylomes have thus far only been generated for sponges and sea anemones (discussed below) (*20*), leaving numerous open questions as to the quantity, genomic localization, and function of nonvertebrate 5hmC.

While it is well established that nonvertebrate genomes exhibit low 5mC, it is worth noting that cis-regulatory elements frequently reside within highly methylated gene bodies. It is thus possible that the 5mC state of these elements is regulated independently of bulk gene body 5mC. For example, we have recently shown that the European lancelet (*Branchiostoma lanceolatum*), an invertebrate chordate, exhibits developmental DNA demethylation of cis-regulatory elements located within methylated gene bodies (*29*). Notably, this demethylation event coincided with the expression of the lancelet TET ortholog, thereby suggesting that animals with mosaic 5mC might use TET-mediated demethylation of enhancers for their spatiotemporal regulation during development. 5hmC profiling of genomic DNA extracted from the demosponge *A. queenslandica* demonstrated enrichment of this mark at potential transcription factor binding sites (*20*). Nevertheless, definitive proof that TET proteins and active DNA demethylation participate in developmental enhancer or promoter usage in nonvertebrate lineages has not been provided to date. To better understand the evolution of TET-mediated regulation of distal regulatory elements, we conducted detailed analyses of genome-wide 5mC and 5hmC dynamics during development of the purple sea urchin (*Strongylocentrotus purpuratus*), which forms part of the sister lineage to chordates, the ambulacrarians (*30*), and the invertebrate chordate European lancelet (*29*). Specifically, we used whole-genome bisulfite sequencing (WGBS) (*31*) and Apolipoprotein B mRNA editing enzyme, catalytic polypeptide (APOBEC)-coupled epigenetic sequencing (ACE-seq) (*32*) to generate base-resolution maps of 5mC and 5hmC, respectively, at four developmental time points. Integration of these datasets with open chromatin profiles demonstrated prominent active DNA demethylation of regulatory regions in both examined organisms, thus strongly supporting the notion that invertebrate deuterostomes use TET proteins and 5hmC for developmental gene regulation. Moreover, we found that vertebrate orthologs of genes marked by 5hmC in these animals are associated with 5hmC enrichment and defined spatiotemporal regulatory logic in zebrafish. Together, our work demonstrates that at least in some nonvertebrate lineages, 5mC is not merely a by-product of gene activity required for the prevention of spurious transcriptional initiation but a bona fide regulatory mark that is being actively remodeled at regulatory regions associated with key developmental processes.

RESULTS

Structural and functional conservation of TET enzymes

To better understand the evolutionary conservation of 5hmC and TET expression dynamics during embryogenesis, we first wanted to determine whether echinoderm and cephalochordate TET enzymes are characterized by the same protein domain composition as vertebrate TETs. The sea urchin genome (*30*) as well as the genomes of the European (*29*) and Florida lancelet (*33*) encode a single copy of TET proteins. The genomes of most vertebrates, however, exhibit two or three TET copies (fig. S1A) (*34*, *35*), which arose during the process of whole-genome duplication (*36*). Comparison of TET protein structure revealed that both the sea urchin TET (sTET) and the lancelet TET (bTET) contain an N-terminal CxxC domain, which is also present in vertebrate TET1 and TET3 enzymes (Fig. 1A) (*37*). CxxC domains can interact directly with the DNA thereby facilitating TET interaction with chromatin (*38*, *39*). The C terminus of sTET and bTET is characterized by a double-stranded β helix (DSBH) domain that harbors binding sites for the Fe(II) and 2-oxoglutarate cofactors required for TET enzymatic activity (*37*). Notably, the DSBH domain in sTET, bTET, and vertebrate TET proteins is interrupted by a sizable low- complexity region (Fig. 1A). These results are in line with the previously described structural conservation of metazoan TET proteins (*24*). We next conducted multiple sequence alignment analyses and found strong sequence conservation in the core catalytic domain (Fig. 1B and fig. S1B), as well as notable structural conservation between sTET, bTET, and their vertebrate counterparts (Fig. 1C and fig. S1, C to E). Having determined the suitability of sea urchin and lancelet for TET evolutionary comparisons and 5hmC profiling, we next quantified TET expression during sea urchin, lancelet, and zebrafish development (*29*, *40*). In all examined species, the developmental peak of TET expression could be observed during mid-development (Fig. 1D), coinciding with gastrulation (sea urchin) and segmentation (lancelet and zebrafish) (fig. S1F) (*41*, *42*). These observations are in accord with reduced developmental requirements for TET activity during vertebrate pluripotency (*10*–*12*, *14*). Overall, our results demonstrate highly conserved TET protein structure and developmental TET expression profiles across diverse deuterostomes, suggestive of the important roles these proteins might play during animal development.

DNA methylation content and dynamics of sea urchin and lancelet genomes

To quantify the amount of genomic 5mC, which can act as substrate for TET oxidation and 5hmC formation, we generated base-resolution 5mC profiles (WGBS) (*31*) corresponding to the following stages of sea urchin development: 24 hours post fertilization (hpf) (blastula), 48 hpf (gastrula), 72 hours post fertilization (hpf) (pluteus), and adult (tube feet). In addition, we analyzed WGBS datasets of lancelet embryogenesis from 8 hpf (blastula, G3), 15 hpf (gastrula, G6), 36 hpf (neurula, T0), and adult (liver, A) time points (Fig. 2A and table S1) (*29*, *41*, *42*). In agreement with previous studies (*29*, *43*), average methylation values (sea urchin = 23 to 28% and lancelet = 21 to 25%) (Fig. 2A) were consistent with canonical invertebrate methylome patterns, where the majority of genomic 5mC is located within gene bodies of expressed genes (fig. S2, A to D) (*17*). Notably, the adult samples of both sea urchin and lancelet displayed considerably lower 5mC levels reminiscent of developmental 5mC dynamics in zebrafish and *Xenopus tropicalis* (Fig. 2A and fig. S2E) (*11*). Given the positive correlation between gene expression and gene body 5mC in nonvertebrate organisms, lower 5mC levels in adult tissues could potentially be explained by specialized transcriptional profiles of those tissues characterized by a smaller number of expressed genes or a lower transcriptional output overall. To that end, we analyzed the transcriptomes (*29*, *40*) of multiple developmental stages and adult tissues and revealed comparable mean expression profiles across all examined samples in both organisms (Fig. 2B). These results suggest that the observed loss of 5mC in adults is likely not caused by major changes in transcriptional complexity but is rather linked to a gradual increase in chromatin accessibility associated with more frequent usage of cis-regulatory elements (*44*). In line with these results, we could not detect any major developmental down-regulation of sea urchin and lancelet DNMT transcripts in adult tissues (fig. S2F). Notably, both sea

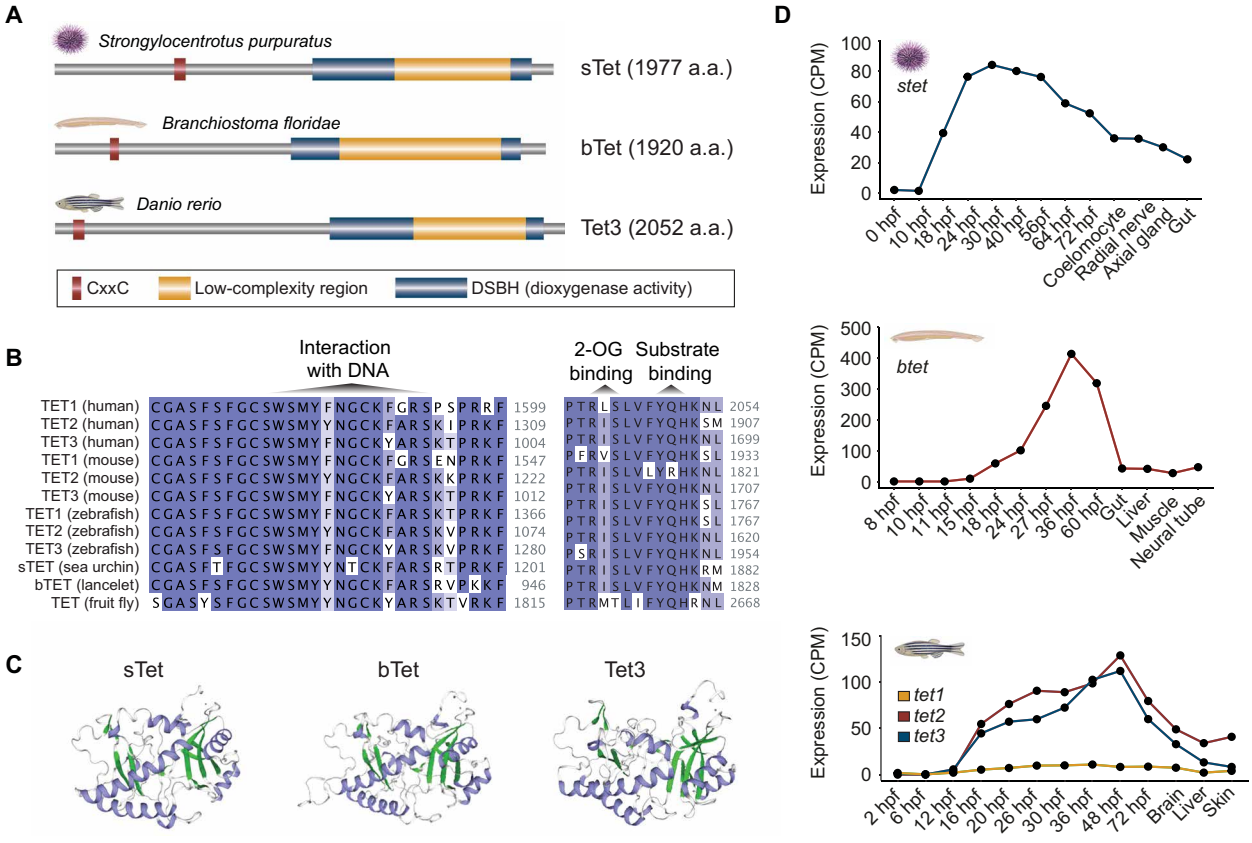

Fig. 1. Evolutionary conservation of TET protein sequence, catalytic domain structure, and developmental expression. (**A**) Sea urchin, lancelet, and zebrafish TET protein domain structure predicted using SWISS-MODEL and HMMER. Sea urchin sTet, Florida lancelet bTet, and zebrafish Tet3 harbor an N-terminal DNA binding CxxC domain and a C-terminal catalytic DSBH domain containing a large low-complexity insert. (**B**) Multiple sequence alignments of human, mouse, and zebrafish TET1, TET2, and TET3 as well as sea urchin, lancelet, and fruit fly TET core catalytic domain. A part of DSBH is shown. The color of each amino acid indicates percentage identity (PID) with darker blue depicting higher PID and lighter blue depicting lower PID. (**C**) Three-dimensional models of methylcytosine dioxygenase domains of sea urchin sTet, lancelet bTet, and zebrafish Tet3 performed using SWISS-MODEL. Crystal structure of the human TET2-5fC complex (5d9y.1.A) was ranked as a top template in the template search and was used for model building. α Helix is depicted in blue, and β sheet is depicted in green. (**D**) TET gene expression dynamics during sea urchin, lancelet, and zebrafish development. a.a., amino acids; 2-OG, 2-oxoglutarate. CPM, counts per million.

urchin and lancelet DNMTs are characterized by a high degree of structural conservation to vertebrates, as described previously (*45*–*49*). To obtain further insight into the developmental dynamics of 5mC, we identified genomic regions, which display significant (false discovery rate < 0.05, ΔmCG/CG ≥ 0.2) developmental changes in 5mC levels (Fig. 2C and tables S2 to S7). We identified 20,072 and 8136 of such differentially methylated regions (DMRs) in sea urchin and lancelet genomes, respectively, with the majority corresponding to the larva/pluteus-to-adult transitions (Fig. 2D and fig. S2G). The majority (86% sea urchin and 80% lancelet) of the identified DMRs were associated with developmental hypomethylation (Fig. 2, C and D, and fig. S2G). These results agree with the overall lower levels of 5mC in adult tissues in both organisms (Fig. 2A). Together, we find that the embryogenesis of sampled invertebrate deuterostomes is characterized by a notable developmental loss of 5mC, which cannot be explained by developmental changes in transcriptional activity or DNMT expression.

Developmental dynamics of the 5hmC landscape

To explore the developmental dynamics, genomic content, and distribution of 5hmC in sea urchin and lancelet genomes and to compare those against vertebrate 5hmC patterns, we used nondestructive, base-resolution sequencing of 5hmC using a DNA deaminase (ACE-seq) (*32*). We first wanted to test how ACE-seq 5hmC quantification compares to TET-assisted bisulfite sequencing (*50*) and immunoprecipitation (hMeDIP-seq) (*51*) 5hmC profiles in zebrafish, an organism with a well-described DNA hydroxymethylome (*11*). First, we found that the same genomic regions displayed 5hmC enrichment identified by all the three techniques (fig. S3, A and B). Furthermore, we observed a robust overlap between data originating from the two base-resolution approaches (fig. S3C) and hence proceeded to generate sea urchin and lancelet 5hmC maps using ACE-seq. We obtained DNA hydroxymethylome profiles for the following stages of sea urchin and lancelet embryogenesis: 24 hpf (blastula), 48 hpf (gastrula), 72 hpf (pluteus), adult (tube feet), and 36 hpf (late neurula, T0), 60 to 72 hpf (larvae, L0), 3 to 4 months (juvenile, J), and adult (liver, A) (table S1) (*41*, *42*). Identification of significantly hydroxymethylated sites (proportion test, *P* adj. < 0.05, ΔhmCG/CG ≥ 0.1) (*52*) in sea urchin and lancelet genomes revealed 1 to 2% of CpGs with significant 5hmC content (Fig. 3A). In zebrafish 24-hpf embryos, which are characterized by strong TET activity (Fig. 1D), ~5% of overall CpGs were identified as significantly

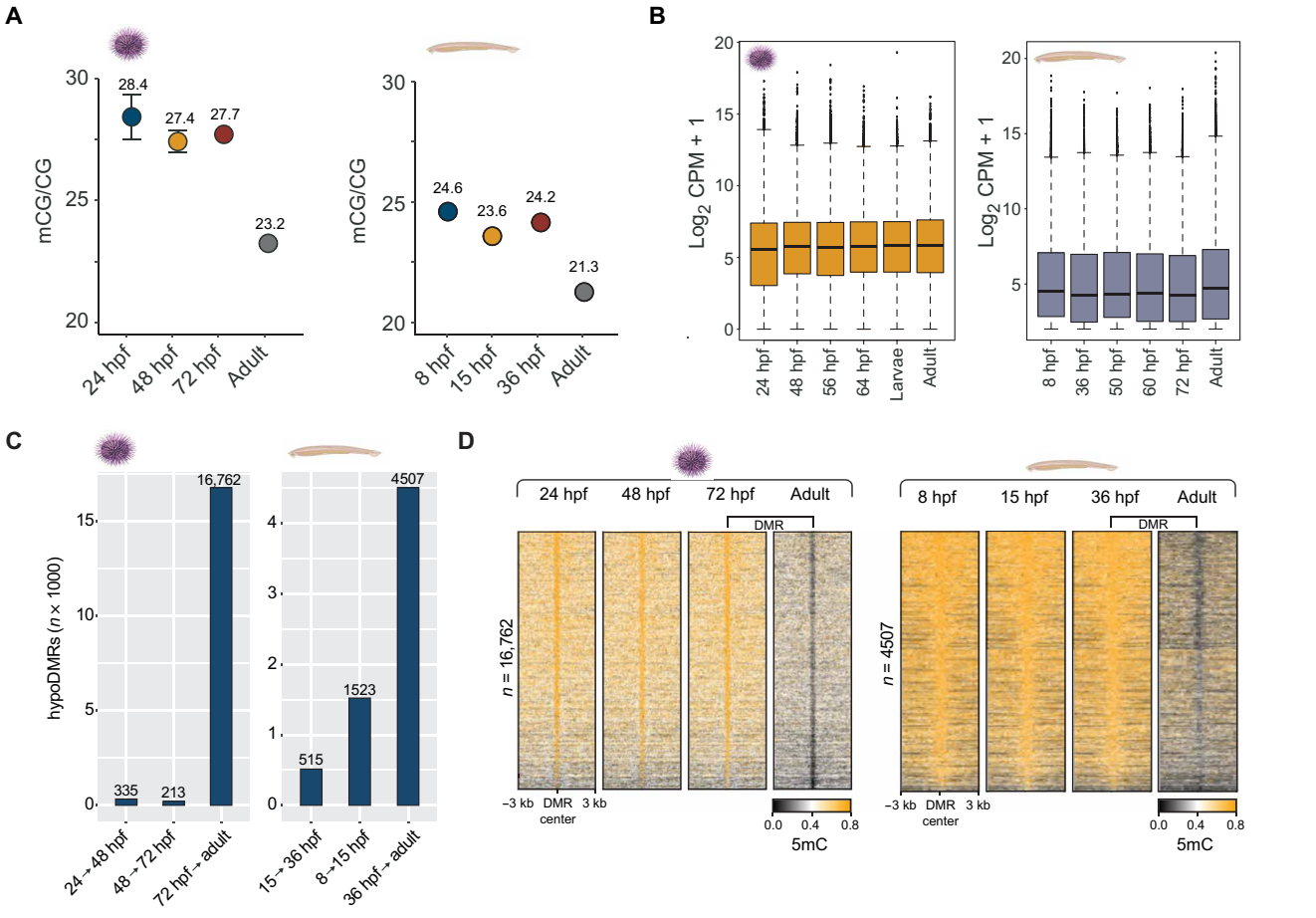

Fig. 2. DNA methylation dynamics of sea urchin and lancelet development. (**A**) Average DNA methylation (mCG/CG) levels during sea urchin and lancelet development. (**B**) Average gene expression (CPM + 1) levels during sea urchin and lancelet development. (**C**) Number of hypomethylated DMRs (hypoDMRs) identified between embryonic and adult stages in sea urchin and lancelet genomes. (**D**) Heatmaps depicting DNA methylation (mCG/CG) at adult hypoDMRs in sea urchin and lancelet genomes.

hydroxymethylated (Fig. 3A). These results are in line with the overall higher global 5mC content of vertebrate genomes (Fig. 3A). To assess the reproducibility of ACE-seq 5hmC data between replicates, we searched the genome for sites of significant 5hmC enrichment and plotted mean 5hmC values between replicates (Fig. 3B). We observed an overall positive correlation of 5hmC levels in those regions with correlation values of $R = 0.58$ and $R = 0.68$ for sea urchin and lancelet, respectively. Given the transient nature of 5hmC and its role in 5mC-to-C conversion, the expectation would be for most of the 5hmC sites to exist in a fully methylated (5mC) state before the onset of TET activity and in a fully demethylated (C) state once the period of TET-mediated demethylation has ended. To test whether this holds true in amphioxus and sea urchin genomes, we identified significant 5hmC sites at the stage coinciding with high TET expression (48 hpf, sea urchin; 60 hpf, lancelet) and interrogated their fate before and after this period (Fig. 3, C and D). Expectedly, we found that most of the hydroxymethylated CpGs were in the 5mC state before the mid-developmental period. The same fraction also displayed a notable enrichment in unmethylated cytosines in adult tissues, in agreement with developmental 5mC removal. These data thus demonstrate that ACE-seq can accurately detect 5hmC at base resolution in sea urchin and lancelet genomes and that 5hmC displays comparable developmental dynamics across deuterostomes.

5hmC-marked regulatory regions in deuterostome genomes

Next, we wanted to assess to what extent does 5hmC correlate with sites of developmental hypomethylation and regulatory regions in general, identified through open chromatin profiling. We first plotted the 5hmC signal over previously identified adult hypomethylated DMRs (Fig. 2) and found a notable overlap between the two datasets (fig. S3D). Of 16,753 DMRs, 5585 (33%) formed a 5hmC-enriched cluster in the sea urchin, whereas in the lancelet, that overlap was 46% (2072 of 4507 DMRs). To obtain more comprehensive insight into the relationships between 5hmC and gene regulation, we generated open chromatin profiles Assay for Transposase Accessible Chromatin with high-throughput sequencing (ATAC-seq), corresponding to 48 hpf (sea urchin) and 60 hpf (lancelet) (*29*) stages (Fig. 3, E and F), which are associated with peaks of TET activity (Fig. 1D). *K*-means clustering ($k = 2$) of 5hmC signal over those regions revealed a subset (cluster 1), which was enriched for 5hmC (Fig. 3, E and F). This cluster was characterized by high 5mC levels in embryonic and low 5mC levels in adult tissues, in agreement with active demethylation occurring at these regions. 5hmC was highly enriched in 48- and 60-hpf embryos in sea urchin and lancelet, respectively, and was almost undetectable in adult samples, as expected from the low 5mC signal in those tissues (Fig. 3, E to G, and fig. S3E). Moreover, analysis of publicly available ATAC-seq data

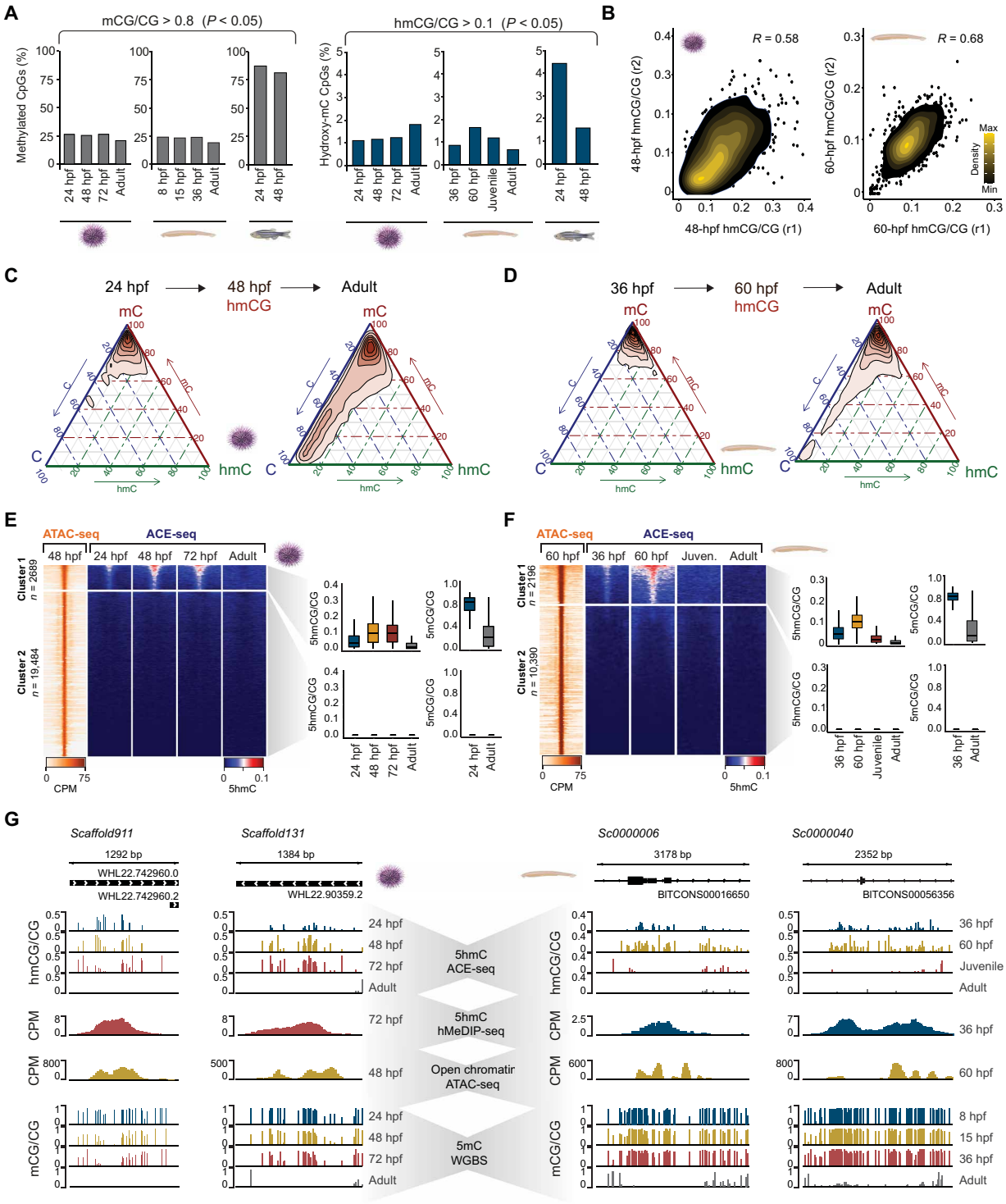

Fig. 3. DNA hydroxymethylation landscape of sea urchin and lancelet development. (**A**) Percentage of methylated and hydroxymethylated CpGs in embryonic and adult tissues of sea urchin, lancelet, and zebrafish. CpG sites with at least 80% methylation and CpG sites with at least 10% hydroxymethylation (P adj. < 0.05) were included in the analysis. Only CpG sites with a minimum of 10× coverage were considered. (**B**) Concordance of hydroxymethylation levels between biological replicates. Sea urchin 48-hpf and lancelet 60-hpf samples are shown. (**C** and **D**) Ternary plots depicting the relationship between methylated (mC), hydroxymethylated (hmC), and unmethylated (C) CpG states in sea urchin (C) and lancelet (D) embryos and adult tissues. CpG sites hydroxymethylated at 48 hpf in sea urchin (C) and 60 hpf in lancelet (D) (P adj. < 0.05, proportion test) are shown. (**E** and **F**) Heatmaps depicting DNA hydroxymethylation dynamics (ACE-seq) of open chromatin regions (ATAC-seq) in sea urchin (E) and lancelet (F). K-means clustering (k = 2) of ACE-seq and ATAC-seq signal over ATAC-seq peaks. Boxplots of DNA hydroxymethylation and DNA methylation dynamics during sea urchin (E) and lancelet (F) development. (**G**) Integrative genomic viewer (IGV) browser tracks depicting DNA hydroxymethylation (ACE-seq and hMeDIP-seq) enrichment at open chromatin regions (ATAC-seq) coinciding with DNA demethylation (MethylC-seq) in sea urchin and lancelet genomes.

corresponding to multiple stages of lancelet development (*29*) uncovered a notable increase in chromatin accessibility at 60 hpf, coinciding with the strongest 5hmC signal (fig. S3, D and F). To define what proportion of 5hmC-marked regions reside in open chromatin, we performed ACE-seq peak calling (see Materials and Methods) and plotted ATAC-seq signal over these peaks. The data revealed an enrichment of open chromatin at ~30 and ~ 60% of ACE-seq peaks in sea urchin and lancelet, respectively (fig. S3G), thereby suggesting that a considerable proportion of 5hmC-marked DNA coincides with putative regulatory regions. Together, these results demonstrate strong 5hmC presence at invertebrate regulatory regions, which coincides with the active removal of 5mC.

5hmC and developmental gene activation

Having characterized developmental dynamics of 5hmC (Fig. 3), we next sought to understand which gene groups are potentially regulated by 5hmC and what impact might 5hmC have on developmental gene regulation. We first generated Gene Ontology profiles (*53*) of genes associated with 5hmC-marked ATAC-seq peaks (*54*) and found significant enrichment for developmental processes (Fig. 4A). Many of these processes such as "system development," "cell differentiation," "tissue development," "developmental process," and others were identical to those associated with 5hmC-regulated genes previously described in zebrafish, *Xenopus*, and mouse embryos (*11*). We then assessed the genomic distribution of 5hmC enrichment and found that most of the 5hmC peaks reside in gene bodies, although a significant fraction of 5hmC was observed in promoters and intergenic regions (Fig. 4B). In line with their proposed developmental function, genes with both promoter and gene body 5hmC peaks were, on average, longer, suggestive of their increased regulatory potential (Fig. 4C and fig. S4, A and B) (*55*). Transcription factor binding motif analyses revealed significant enrichment for Sox- and Fox-binding sites, both of which have been previously shown to associate with TET proteins and DNA demethylation in vertebrates (Fig. 4D; fig. S4, C and D; and tables S8 to S13) (*56*, *57*). In vertebrates, promoter 5hmC is linked to transcriptional activation (*58*). To test whether a similar association could be reproduced in sea urchin and lancelet genomes, we analyzed the transcriptional profiles of genes with a promoter 5hmC peak and found that promoter 5hmC correlates with activation of developmental genes in both examined organisms (Fig. 4E). Accumulation of 5hmC at gene promoters and activation of corresponding gene expression coincided with gradual reduction of 5mC during development (figs. S4E and S5), as demonstrated through examples of developmental gene activation in the sea urchin (*Tjp1* gene; fig. S5, A, C, and E) and the lancelet (*Blimp1* gene; fig. S5, B, D, and E). A similar positive correlation between 5hmC and transcription was also observed at genes with gene body 5hmC peaks; however, this effect was less pronounced, likely because of challenges in associating distal 5hmC peaks with their target genes (fig. S4F). To explore the effect of 5hmC on the expression of developmental genes in more detail, we focused on sea urchin and lancelet orthologs of fruit fly developmental genes defined by Gene Ontology. Similar to vertebrates, where many key developmental genes belonging to Hox or Fox families are located within hypomethylated Polycomb-marked DNA methylation valleys (*59*), we found that these genes also hypomethylated in sea urchin and lancelet throughout development (fig. S6, A to E). Overall, we found that 19.2% (n = 389) of developmental genes in sea urchin and 43.3% (n = 1272) in lancelet are hypomethylated (fig. S6A). Of the remaining, whose gene bodies are methylated, 12.5% (n = 205) and 9.5% (n = 158) harbor 5hmC-ATAC elements in sea urchin and lancelet, respectively. Thus, as in vertebrates (*11*, *60*), only a fraction of developmental genes in both sea urchin and lancelet display 5hmC-mediated regulation. In sum, these results provide proof for the presence of 5hmC at regulatory regions of a subset of developmental genes in invertebrate deuterostome genomes and suggest that active removal of 5mC through the 5hmC intermediate might play a role in their activation.

Conserved regulatory logic of 5hmC-marked genes

Previously, we have described widespread TET-mediated demethylation of regulatory regions during the vertebrate phylotypic period, which can be defined as the most conserved stage of vertebrate embryogenesis (*11*). These phylotypic DMRs (phylo-DMRs) coincided with developmental DNA demethylation and were marked by 5hmC in zebrafish, *Xenopus*, and mouse embryos. To explore the extent to which genes regulated by 5hmC in invertebrate deuterostomes coincide with genes linked to vertebrate 5hmC, we first identified zebrafish orthologs of 5hmC-marked genes in sea urchin and lancelet, defined their regulatory landscapes (*54*), selected the zebrafish orthologs enriched in 5hmC, and assessed their overlap (fig. S7A). This analysis resulted in 148 and 343 zebrafish 5hmC-marked genes, which overlapped lancelet and sea urchin 5hmC-marked genes, respectively. Having identified this notable agreement in 5hmC regulation, we next wanted to study in more detail the regulatory logic behind 5hmC gene marking. Both whole-genome and local duplication events act as a driving force of the evolutionary novelty by supplying new genetic material, which has the potential to evolve divergent regulatory functions (*61*). We, therefore, wanted to compare spatial and temporal expression profiles of zebrafish gene ohnologs, which arose after three rounds of whole-genome duplication in teleost fishes, with and without 5hmC-ATAC–marked regulatory elements. To that end, we selected all zebrafish orthologs of sea urchin 5hmC-marked genes and identified a list of their 2R/3R ohnologs using OHNOLOGS v2 resource (*62*). We then stratified ATAC-seq–associated regulatory elements in the zebrafish genome within each ohnolog gene's landscape (*54*) into three categories depending on phylo-DMR presence and 5hmC enrichment (fig. S7B): group 1 (ATAC-seq peaks overlapping a phylo-DMR and displaying 5hmC enrichment), group 2 (ATAC-seq peaks displaying 5hmC enrichment without phylo-DMR overlap), and group 3 (ATAC-seq peaks without 5hmC enrichment or phylo-DMR overlap). We only retained zebrafish genes that had ohnologs in at least two of the aforementioned groups. We next analyzed the transcriptional profiles of zebrafish orthologs linked to these three groups and found that phylo-DMR–linked genes (group 1) were characterized by peaks of expression surrounding the phylotypic period (24 hpf), whereas 5hmC-marked genes without phylo-DMR association (group 2) were developmentally up-regulated at later embryonic stages (48 to 72 hpf) and exhibited the strongest expression in the adult brain (Fig. 5A). Genes that were not enriched in 5hmC or phylo-DMRs (group 3) did not display such notable developmental dynamics (Fig. 5A). To obtain further insight into the spatiotemporal regulation of these orthologs, we analyzed single-cell resolution transcriptomes of the zebrafish phylotypic-stage embryo (24 hpf) (Fig. 5B) (*63*). We found that group 1 genes were expressed broadly in cell types originating from diverse embryonic layers, whereas group 2 genes were expressed predominantly in neurons,

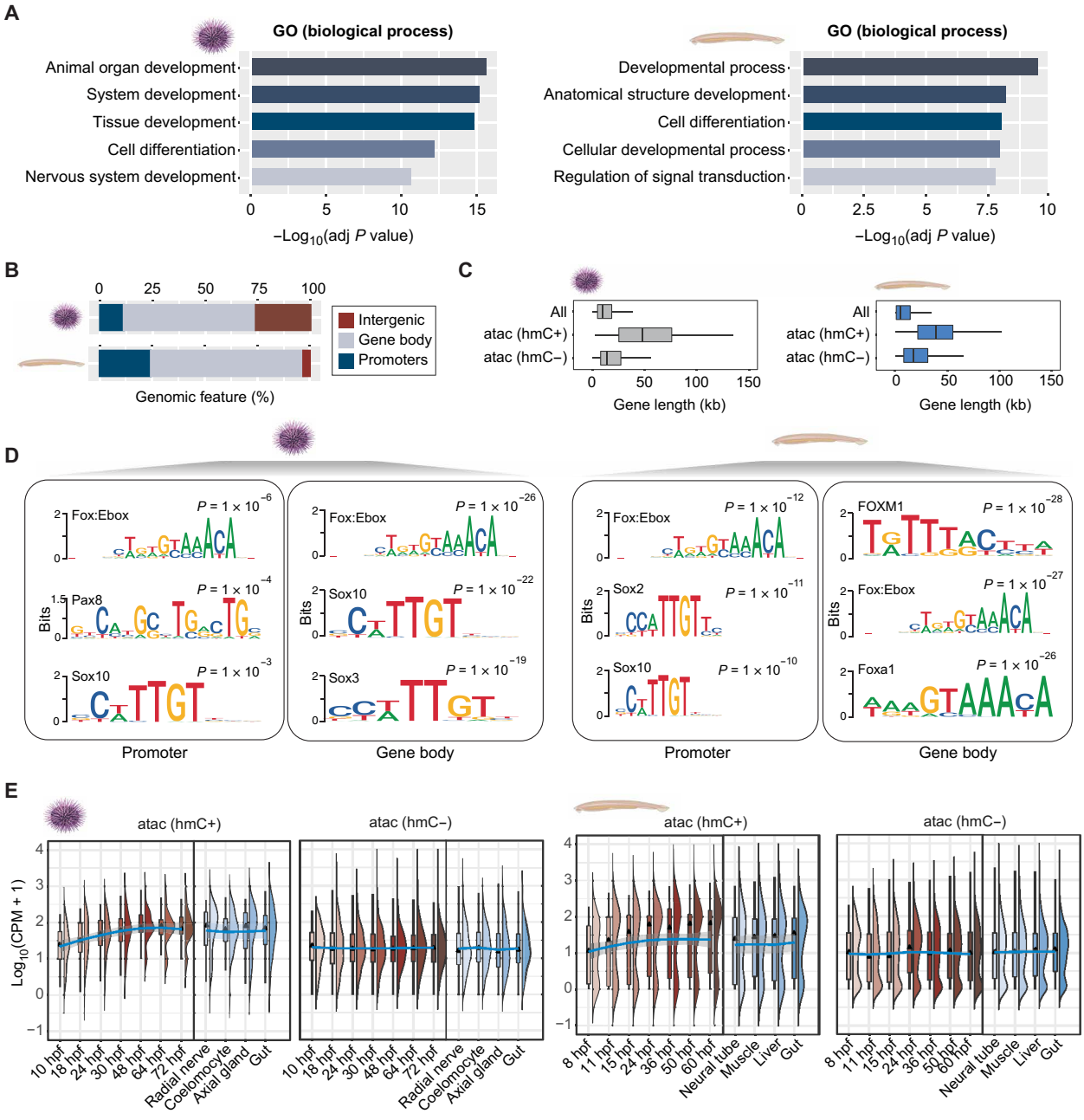

Fig. 4. Developmental expression of 5hmC-marked genes. (**A**) Gene Ontology (GO) analysis of genes harboring 5hmC-marked ATAC-seq peaks at their promoters or gene bodies in sea urchin and lancelet. (**B**) Percentage of 5hmC-marked ATAC-seq peaks at different genomic regions. (**C**) Length of the genes harboring promoter-associated 5hmC-marked ATAC-seq peaks (promoter atac hmC+) and non-5hmC ATAC-seq peaks (promoter atac hmC−). (**D**) HOMER motif enrichment analysis of atac hmC+ regions associated with either gene promoters or gene bodies. (**E**) Expression dynamics of promoter atac hmC+ genes as compared to promoter atac hmC- genes in sea urchin and lancelet embryos and adult tissues.

in line with their bulk RNA sequencing (RNA-seq) expression profile (Fig. 5, A to C, and fig. S7C). Group 3 orthologs were characterized by a minor enrichment in the erythroid lineage. Given the strong link between 5hmC and loss of 5mC in nonvertebrate (Fig. 2) and vertebrate (*11*) adult tissues, we next sought to interrogate the 5mC state of these three groups of regulatory elements in adult zebrafish (Fig. 5D) (*64*). Our data demonstrate that both 5hmC-enriched ATAC peaks with and without phylo-DMR association are predominantly hypomethylated in most adult tissues (Fig. 5D). Unlike group 2 elements, which are exclusively hypomethylated in adults, group 1 elements were already hypomethylated during the phylotypic period. Last, group 3 elements that displayed no 5hmC enrichment coincided with peaks of broad and pervasive hypomethylation characteristic of CpG islands (*65*). These data argue that most invertebrate 5hmC-marked genes also display an association with this regulatory mark in vertebrates and that vertebrates use 5hmC during organogenesis (group 1 elements) as well as during later stages of tissue differentiation (group 2 elements). We then

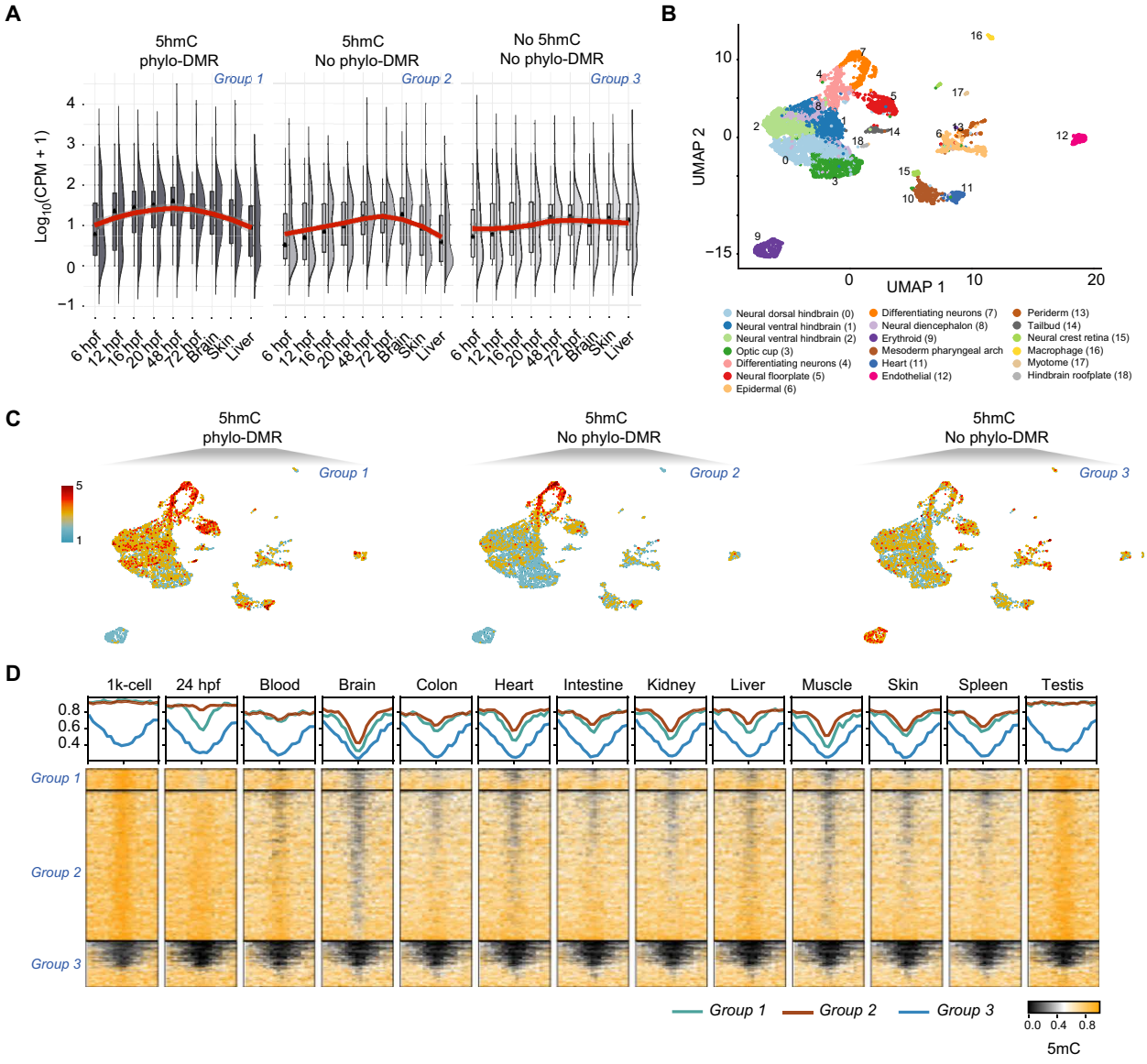

Fig. 5. Conservation of developmental regulatory logic of 5hmC-marked genes in zebrafish. (**A**) Expression of 2R/3R-ohnolog zebrafish genes associated with either 5hmC-marked ATAC-seq peaks overlapping phylo-DMRs (5hmC/phylo-DMR), 5hmC-marked ATAC-seq peaks not overlapping phylo-DMRs (5hmC/no phylo-DMR), or non-5hmC ATAC-seq peaks not overlapping phylo-DMRs (no 5hmC/no phylo-DMR) in embryos and adult tissues. (**B**) Uniform manifold approximation and projection (UMAP) projection of 7738 individual cells from the 24-hpf zebrafish embryo. Cells are color-coded by tissue types. (**C**) *Z*-transformed module scores of three gene sets: 5hmC/phylo-DMR, 5hmC/no phylo-DMR, and no 5hmC/no phylo-DMR in 24-hpf zebrafish embryo. Module scores depict the difference between the average gene expression of each gene set and random control genes. (**D**) Heatmaps showing DNA methylation profiles of 5hmC/phylo-DMR, 5hmC/no phylo-DMR, and no 5hmC/no phylo-DMR ATAC-seq peaks in 1k-cell and 24-hpf zebrafish embryos as well as multiple adult tissues.

performed the reverse analysis, where we analyzed developmental expression dynamics of sea urchin and lancelet genes orthologous to zebrafish genes, which harbor ATAC-seq peaks overlapping a phylo-DMR and displaying 5hmC enrichment (5hmC/phylo-DMR) in their distal regulatory domains. We compared these dynamics to those of sea urchin and lancelet genes orthologous to zebrafish genes, which harbor ATAC-seq peaks displaying 5hmC enrichment without phylo-DMR overlap (5hmC/no phylo-DMR) or ATAC-seq peaks without 5hmC enrichment or phylo-DMR overlap (no 5hmC/no phylo-DMR). The analysis revealed a trend toward developmental activation, which was particularly notable for sea urchin genes, whose zebrafish orthologs harbor 5hmC/phylo-DMRs (fig. S8, A and B), thus further supporting the finding of the conserved regulatory logic of 5hmC-marked genes.

DISCUSSION

The goal of the current study was to explore the evolutionary conservation of TET-mediated DNA demethylation in nonvertebrate lineages by generating base-resolution profiles of developmental 5hmC landscape dynamics. First, we have shown that the expression of sea urchin and lancelet TET orthologs by and large resembles

anamniote TET developmental expression profiles, which are characterized by peaks of TET activity during mid-development (phylotypic period) (*11*). While TET proteins play important roles in mammalian pluripotency and reprogramming in vitro (*13*, *58*, *66*), mouse triple TET knockouts developed normally until gastrulation (*10*) indicative of reduced requirements for TET activity during in vivo pluripotency. Similarly, zebrafish homozygous TET knockouts generated by transcription activator-like effector technology (TALE) (*14*) or CRISPR-Cas9 F0 mutants (*12*) and morphants (*11*), all displayed developmental defects only during later embryonic stages. Our results thus suggest that active DNA demethylation removal and likely 5mC in general are not required for the establishment of deuterostome pluripotency.

While the members of TET/JBP (J-protein binding) family have been identified across all domains of life, ranging from viruses to humans (*24*), fairly little is known regarding the functions of these proteins in DNA demethylation beyond vertebrates (*17*, *26*, *28*). For example, in *Drosophila*, the single identified TET ortholog has only been associated with RNA hydroxymethylation (*25*), whereas detailed, base-resolution invertebrate 5hmC maps have thus far only been generated for the demosponge *A. queenslandica* and the sea anemone *Nematostella vectensis* (*20*). However, in *A. queenslandica*, 5hmC was detectable at identical positions during embryonic and larval stages without displaying any signs of developmental loss (*17*). This suggests that *A. queenslandica* either uses 5hmC as a stable gene-regulatory mark or that TET-mediated DNA demethylation occurs during later developmental transitions. In this work, we conclusively demonstrate that genomic sites of 5hmC enrichment coincide with developmental 5mC loss and the presence of accessible chromatin, in line with the proposed roles of TET proteins and 5hmC in gene regulation (*67*). Specifically, we detect 5hmC at both proximal and distal regulatory regions and show that 5hmC presence and developmental loss of 5mC coincide with the activation of developmental genes. One plausible mechanism by which 5hmC and TET proteins could participate in developmental gene regulation is through locus-specific TET recruitment by pioneer factors such as forkhead box A1 (FOXA1) (Fig. 4D). FOXA1 and similar pioneer factors could recruit TET (*57*) to methylated and inaccessible cis-regulatory regions and promote demethylation of the targeted locus to render it more accessible to methylation-sensitive transcription factors (*68*). Accumulation of these activating transcription factors would then lead to chromatin opening of the regulatory sequence and the activation of its linked gene. In line with this hypothesis, it was previously demonstrated in zebrafish (*11*) and mammals (*69*) that TET depletion has a negative impact on chromatin accessibility of distal regulatory elements. Furthermore, here, we show that the 5hmC signal is strongest in 60-hpf lancelet embryos, which coincides with the developmental point of highest chromatin accessibility. Collectively, these data suggest that TET proteins and 5hmC participate in chromatin opening at developmental gene-regulatory regions across the animal kingdom.

We have previously demonstrated that active DNA demethylation of enhancers associated with key developmental pathways is a hallmark of vertebrate development (*11*). Here, we further expand on these observations to conclude that TET activity and active DNA demethylation of regulatory regions during mid-developmental stages could form a conserved developmental signature of diverse animal phyla. It is worth noting, however, that further work will be needed to validate the role of TET proteins, 5hmC, and active DNA demethylation in the embryonic development of *S. purpuratus* and *B. lanceolatum*. Specifically, future experiments using Cas9/Cas13 technologies (*70*, *71*), will be required to better understand gene-regulatory networks affected by TET loss and to unravel the evolutionarily conserved and species-specific developmental requirements for active DNA demethylation. Furthermore, the current study is limited to invertebrate deuterostomes from the phylum Echinodermata (*S. purpuratus*) and Chordata (*B. lanceolatum*), making it thus challenging to extrapolate our findings beyond these two lineages. Deeply conserved DNA demethylation toolkits consisting of TET proteins and DNA repair machinery as well as canonical gene body 5mC patterns observed in most animals (*17*, *24*) would support widespread usage of TETs and 5hmC for gene regulation. Nevertheless, transcriptome profiling of multiple developmental stages across 10 different phyla demonstrated divergence in the usage of signaling pathways and transcription factors during mid-developmental stages (*72*). It remains to be seen how prevalent TET-mediated regulation of developmental genes is in other animal lineages and whether 5mC/5hmC regulatory logic could be ancestral to bilaterian animals. Last, in the current study, we have shown that 5hmC-regulated genes identified in invertebrate deuterosteomes also display 5mC/5hmC-mediated regulation in the zebrafish genome and that most of these 5hmC-enriched genes are linked to either actively demethylated phylotypic enhancers or regulatory regions that become demethylated. Overall, our study provides novel insight into the 5mC/5hmC regulatory logic beyond the invertebrate-vertebrate boundary and demonstrates that active 5mC removal from regulatory regions during animal development predates vertebrate origins.

MATERIALS AND METHODS

Genomic DNA extraction from sea urchin embryos and adult tissues

S. purpuratus adult animals were collected in the San Diego Bay area, San Diego County, California (USA), and kept in a closed tank system with circulating diluted Mediterranean Sea water at 36 parts per thousand and 14°C at Stazione Zoologica Anton Dohrn. Adult tube feet were collected by surgically removing them from the adult sea urchin attached to a glass beaker with seawater. To obtain embryos and larvae, sea urchin gametes were collected by vigorously shaking the adults. Eggs were collected by placing the sea urchin aboral side up onto a beaker filled with seawater. Sperm was collected with a p200 micropipette into a 1.5-ml tube, which was placed on ice. The eggs were filtered once through a 100-μm mesh filter to remove debris. Five microliters of sperm was diluted in 13 ml of seawater, and then 20 drops of this dilution were added to the eggs to fertilize them. Fertilized eggs were incubated in seawater at 15°C until the desired stage. Twenty-five to 50 μl of sea urchin larvae or embryos were collected for DNA extraction using a 40-μm mesh filter and placed into 1.5-ml tubes. Tubes with adult tube feet, embryos, and larvae were centrifuged at 500*g*, and the supernatant was discarded. The resulting pellets were frozen by placing the tubes in liquid nitrogen and then stored at −80°C until further processing. The DNA extraction procedure was identical for sea urchin adult tube feet, embryos, and larvae. The frozen pellet was washed three times with 1× SSC in Milli-Q H_2O by centrifuging at 500*g* for 5 min and removing the supernatant. The washed pellet was resuspended in 750 ml of lysis buffer [10 mM tris (pH 7.5), 1 mM EDTA, 1% SDS, 3.4% β-mercaptoethanol, and proteinase K (660 μg/ml)] and

incubated at 56°C for 2 hours at 300 rpm in a heat block. After cooling down an equal amount of phenol/chlorophorm/isoamylalcohol (mixture in 25:24:1 proportion at neutral pH) was added and mixed by inverting the tube several times, followed by centrifugation at 16,000*g* for 10 min at 4°C to separate the phases. The top phase was collected and mixed with an equal volume of chloroform/isoamyl alcohol (mixture in 24:1 proportion). The solution was mixed by inversion and centrifuged at 16,000*g* for 10 min at 4°C. The top phase was collected and combined with 0.1 volume of 3 M NaAc (pH 5.0) and two volumes of ice-cold 100% EtOH. The solution was mixed by inverting the tube several times. Precipitated DNA was collected by a p20 micropipette and placed in a 1.5-ml tube with 200 μl of 70% EtOH. This procedure was repeated twice to wash the DNA. The precipitated DNA pellet was then placed into an empty clean 1.5-ml tube and air-dried to remove EtOH. Dried DNA was resuspended in 200 to 500 μl of 1× TE buffer (pH 8.0) depending on the amount of DNA.

Genomic DNA extraction from lancelet embryos and adult tissues

Adults of *B. lanceolatum* were collected at the Racou beach near Argelès-sur-Mer, France (latitude 42°32′53′′ N, longitude 3°03′27″ E) with a specific permission delivered by the Prefect of Region Provence Alpes Côte d'Azur. *B. lanceolatum* is not a protected species. Gametes were obtained after heat stimulation as previously described (*73*) and were used for in vitro fertilization in petri dishes filled with filtered seawater. Embryos were collected at the desired stages and placed in 1.5-ml tubes (at least 500 embryos per tube). The seawater was discarded after 1 min of centrifugation at 13,000 rpm. Adults were immobilized in $MgCl_2$ 7% during 5 min, placed back in seawater, and euthanized by decapitation. The hepatic cecum was dissected and placed in 1.5-ml tubes. The embryos and adult tissues were processed using a DNeasy Blood and Tissue kit (QIAGEN) following the instructions provided by the manufacturer, with an incubation in lysis buffer at 56°C during 5 hours and using 200 μl of elution buffer.

MethylC-seq library preparation

For MethylC-seq library preparation, 1000 ng of genomic DNA was extracted from sea urchin embryos and adult tissues, spiked with unmethylated λ phage DNA (Promega), and sonicated to ~300–base pair (bp) fragments using an M220 focused ultrasonicator (Covaris) with the following parameters: peak incident power, 50 W; duty factor, 20%; cycles per burst, 200; and treatment time, 75 s. Sonicated DNA was then purified, end-repaired using the End-It DNA End-Repair Kit (Lucigen), and A-tailed using Klenow Fragment (3′ → 5′ exo-) (New England Biolabs) followed by the ligation of NEXTFLEX Bisulfite-Seq adapters. Bisulfite conversion of adapter-ligated DNA was performed using the EZ DNA Methylation-Gold Kit (Zymo Research). Library amplification [13 polymerase chain reaction (PCR) cycles] was performed with KAPA HiFi HotStart Uracil+ DNA polymerase (Kapa Biosystems). Library size was determined by the Agilent 4200 TapeStation system. The libraries were quantified using the KAPA library quantification kit (Roche), yielding ~10 to 20 nM. The assays were performed in two biological replicates.

ACE-seq library preparation

ACE-seq library preparation for base resolution 5hmC profiling was performed as previously described (*32*) in two biological replicates. Briefly, 100 ng of genomic DNA extracted from sea urchin, lancelet, and zebrafish embryos and adult tissues was spiked with 1 ng of CpG-methylated λ phage DNA (Wisegene) and 0.5 ng of all-C hydroxymethylated pUC19 plasmid DNA (Wisegene) and sonicated to ~300-bp fragments using an M220 focused ultrasonicator (Covaris), with the following parameters: peak incident power, 50 W; duty factor, 20%; cycles per burst, 200; and treatment time, 75 s. Sonicated DNA (125 μl of total volume) was concentrated to 16.6 μl using AMPure beads (1 volume of DNA : 2 volumes of AMPure beads). 5hmC protection reaction was performed using β-glucosyltransferase (10 U/μl; New England Biolabs) in Cutsmart Buffer according to the manufacturer's instructions at 37°C for 1 hour, followed by 10 min at 65°C. The DNA was denatured in dimethyl sulfoxide at 95°C for 10 min and immediately placed on dry ice for 2 min allowing the samples to freeze. C and 5mC deamination reaction was performed using the APOBEC3A enzyme (NEBNext Enzymatic Methyl-seq Kit, New England Biolabs) with the following ramping conditions: 4°C for 10 min, 4° to 50°C 2:15 min per degree of the ramp, 50°C for 10 min. Deaminated DNA was then purified using AMPure beads (1 volume of DNA: 1 volume of AMPure beads) and subjected to low-input library preparation using an Accel-NGS Methyl-Seq DNA kit (Swift Biosciences). Briefly, DNA was denatured and subjected to an adaptase reaction, followed by primer extension, adapter ligation, and 15 cycles of indexing PCR. Library size and consistency were determined by the Agilent 4200 TapeStation system. The libraries were quantified using the KAPA library quantification kit (Roche).

hMeDIP-seq library preparation

The hMeDIP assay was performed in two biological replicates according to the manufacturer's instructions (Active Motif, hMeDIP, catalog no. 55010) on sea urchin 72-hpf, lancelet 36-hpf, and zebrafish 24-hpf embryos. DNA was sonicated with Covaris to generate ~300-bp fragments. Briefly, 200 to 400 ng of fragmented DNA were spiked with either unmethylated, 5mC-methylated, or 5hmC-hydroxymethylated 338-bp PCR product of APC genomic locus. The DNA was denatured for 10 min at 95°C and immunoprecipitated overnight at 4°C with 4 μl of 5hmC monoclonal antibody (Active Motif, catalog no. 55010). To allow selective enrichment of immune-captured DNA fragments, the mixture was incubated with 25 μl of protein G magnetic beads for 2 hours at 4°C before washing of unbound DNA fragments. Bound hydroxymethylated DNA was eluted, treated with proteinase K, and purified by phenol/chloroform/isoamyl alcohol extraction and ethanol precipitation. hmC-containing DNA was subjected to library preparation using the TruSeq ChIP Sample Preparation kit (Illumina). The specificity of the hMeDIP assay was validated by quantitative PCR of the unmethylated, methylated, and hydroxymethylated spike-in APC controls.

ATAC-seq library preparation

ATAC-seq assays were performed on sea urchin embryos as previously described (*74*) in two biological replicates. For each of the two ATAC-seq replicates, approximately 45,000 cells (corresponding to ~135 embryos at 48 hpf) were lysed in cold lysis buffer [10 mM tris (pH 7.4), 10 mM NaCl, 3 mM $MgCl_2$, and 0.2% NP-40/IGEPAL) after removing the seawater and washing the embryos with filtered ice-cold artificial seawater three times by centrifuging at 500*g*. The resultant nuclei were then incubated for 30 min at 37°C with an in-house made Tn5 enzyme and purified with the QIAGEN MinElute

kit (Qiagen, 28004). PCRs for each replicate were performed with 15 cycles using Ad1F and Ad2.2R primers and NEBNext High-Fidelity 2× PCR Master Mix (New England Biolabs, catalog no. M0541). The resulting libraries were multiplexed and sequenced on HiSeq 4000 lanes.

MethylC-seq data analysis

Sea urchin and lancelet MethylC-seq libraries were sequenced on the Illumina HiSeqX platform [150 bp, paired end (PE)]. Sequenced reads in FASTQ format were trimmed using Trimmomatic (ILLUMINACLIP: adapter.fa:2:30:10 SLIDINGWINDOW:5:20 LEADING:3 TRAILING:3 MINLEN:50). Trimmed reads were mapped to Spur_v3.1, Bl71nemr and danRer10 genome references for sea urchin, lancelet, and zebrafish, respectively, (all containing the λ phage genome as chrLambda) using WALT with the following settings: -m 10-t 24 -N 10000000 -L 2000. Mapped reads in SAM format were converted to BAM and indexed using SAMtools (*75*). Optical and PCR duplicates were removed using Picard Tools function MarkDuplicates REMOVE_DUPLICATES = true (http://broadinstitute.github.io/picard/). Methylated and unmethylated cytosines at each genomic CpG position were called using MethylDackel v0.3.0 (https://github.com/dpryan79/MethylDackel). Additional MethylDackel extract parameters --minOppositeDepth 5 --maxVariantFrac 0.5 were used for the genotype correction (to exclude C-to-T nucleotide transitions). In addition, sequencing read boundaries obtained from MethylDackel mbias were reviewed and fed into MethylDackel extract --OT a,b,c,d, --OB a,b,c,d parameters. For MethylC-seq, bisulfite conversion efficiency was estimated from the λ phage spike-in control. Global DNA methylation at different developmental stages was estimated using two approaches: (i) 5mC/C ratio per single CpG site and averaged across all CpG sites in the genome and (ii) sliding window approach where average 5mC/C was calculated per 10-kbp windows with 2-kbp sliding intervals. Sliding windows were generated using bedtools makewindows -w 10000 -s 2000.

ACE-seq data analysis

Sea urchin, lancelet, zebrafish, and mouse ACE-seq libraries were sequenced on Illumina HiSeqX and NovaSeq 6000 platforms (150 bp, PE). Adapter clipping and read quality trimming was performed using Trimmomatic (ILLUMINACLIP:NEXTflex.fa:2:30:10 SLIDINGWINDOW:5:20 LEADING:5 TRAILING:5 MINLEN:50 CROP:140 HEADCROP:10). These settings allow for the removal of low-complexity Adaptase tails. Trimmed reads were mapped to Spur_v3.1, Bl71nemr, danRer10, and mm10 genome references for sea urchin, lancelet, zebrafish, and mouse (*32*), respectively, (all containing the λ phage genome as chrLambda and pUC19 plasmid genome as chrPUC) using WALT with the following settings: -m 10 -t 24 -N 10000000 -L 2000. Mapped reads in SAM format were converted to BAM and indexed using SAMtools. Optical and PCR duplicates were removed using Picard Tools's function MarkDuplicates REMOVE_DUPLICATES = true. Reads with more than three consecutive nonconverted cytosines in the CC, CA and, CT context were removed using Picard Tools' function FilterSamReads. To determine sequencing read boundaries displaying uniform hydroxymethylation rate and to increase the accuracy of CpG hydroxymethylation calling, we ran the methylation bias command: MethylDackel mbias. The numbers of hydroxymethylated and unmethylated cytosines at each genomic CpG position were called using the MethylDackel extract genome.fasta input.bam -o output --mergeContext. Additional MethylDackel extract parameters --minOppositeDepth 5 --maxVariantFrac 0.5 were used for genotype correction. In addition, sequencing read boundaries obtained from MethylDackel mbias were reviewed and fed into MethylDackel extract --OT a,b,c,d, --OB a,b,c,d parameters. To call ACE-seq peaks, we joined CpG sites with 5hmCG/CG levels 0.1 located within 100 bp of each other in hydroxymethylated regions.

Statistical analysis of hydroxymethylation calling

Statistical analysis of the accuracy of ACE-seq 5hmC calling at a given CpG site was performed following the assumption that the number of "C" reads (N_c) for each CpG site follows a binomial distribution $N_c \sim \text{binomial}(p, n)$ where p (probability distribution) is the 5mC-to-T nonconversion rate and n is sequencing depth (number of "C" + "T" reads per each CpG site). Proportion test (R prop.test) was used to test the null hypothesis H0 that the observed proportion (the number of "C" reads at a given CpG site) equals the expected proportion (p) and the alternative hypothesis H1 that that the observed proportion is greater than the expected proportion. The following parameters were used: prop.test(x, n, p = nonconv_rate, alternative = "greater"), where x is a vector of counts of successes (number of "C" reads for each CpG site), n is a vector of counts of trials (number of "C" + "T" reads per each CpG site, i.e., coverage), p is a vector of probabilities of success (5mC-to-T nonconversion rate). Nonconversion rate of each ACE-seq library was estimated using the M.SssI CpG methyltransferase 5mCG-methylated λ phage spike-in controls. The nonconversion rate is the proportion of "C" reads at methylated CpG sites of the 5mCG λ phage spike-in control being incorrectly retained as cytosines due to inefficient APOBEC3A-mediated deamination of 5mC. The statistical analysis was restricted to CpG sites covered by at least 10 reads.

Identification of DMRs

Differentially methylated CpG sites between consecutive embryonic and adult stages were identified using the DMLtest function of the DSS package. Differentially methylated CpG sites located within 50 bp from each other were joined into regions (DMRs), which were filtered to harbor at least five differentially methylated CpGs that span at least 50 bp. DMRs containing more than 25% of CpGs within them with sequencing coverage less than 5× were excluded from the analysis. The remaining DMRs were defined as hypomethylated or hypermethylated when both replicates displayed at least 20% average methylation difference between consecutive developmental stages.

hMeDIP-seq data analysis

hMeDIP-seq libraries from sea urchin 72-hpf, lancelet 36-hpf, and zebrafish 24-hpf embryos were sequenced on Illumina HiSeq X platform. hMeDIP-seq raw data were processed using the NGSANE framework v0.5.2.0. Briefly, sequenced hMeDIP-seq reads in FASTQ format were trimmed using Trimmomatic (ILLUMINACLIP: TruSeq3-PE.fa:2:30:10 SLIDINGWINDOW:5:20). Trimmed reads were mapped to Spur_v3.1, Bl71nemr and danRer10 reference genomes for sea urchin, lancelet, and zebrafish, respectively, using bowtie2 v2.1.0 with the following parameters: bowtie2 --end-to-end -R 2 -p 10 -N 1 --very-sensitive -X 1000 --no-mixed --no-discordant (*76*). Optical and PCR duplicates were removed using Picard Tools function MarkDuplicates REMOVE_DUPLICATES = true. hMeDIP-seq signal enrichment over ATAC-seq peaks was plotted using deepTools2 computeMatrix reference-point and plotHeatmap functions.

ATAC-seq data analysis

Sea urchin ATAC-seq data were generated as part of this study, whereas lancelet and zebrafish ATAC-seq data were downloaded from GSE106428. Sequenced ATAC-seq reads in FASTQ format were trimmed using Trimmomatic software (ILLUMINACLIP:TruSeq3-PE.fa:2:30:10 SLIDINGWINDOW:5:20 LEADING:3 TRAILING:3 MINLEN:25). Properly paired trimmed read pairs were mapped to Spur_v3.1, Bl71nemr, and danRer10 genome references for sea urchin, lancelet, and zebrafish, respectively, using bowtie2 v2.1.0 with the following parameters: bowtie2 -p 10 -N 1 --very-sensitive -X 2000 --no-mixed --no-discordant. Mapped reads in SAM format were converted to BAM and indexed using SAMtools. Optical and PCR duplicates were removed using Picard Tools function MarkDuplicates REMOVE_DUPLICATES = true. ATAC-seq fragment length distribution was plotted using deeptools2 bamPEFragmentSize --histogram. Removal of mono-, di-, and trinucleosome-bound DNA fragments (and retention of the nucleosome-free fragments) and read adjustment +4 and −5 bp for positive and negative strand, respectively, was performed using deepTools2 alignmentSieve --ATACshift --maxFragmentLength 100. Peaks were called using MACS2 with the following parameters: macs2 callpeak -t $input_bam -f BAMPE -g ${genome_size} --nomodel --nolambda --outdir ${OUTPUT_DIR} -n $name --call-summits -B -q 0.05 (*77*).

RNA-seq data analysis

Sea urchin RNA-seq data were downloaded from PRJNA81157, whereas lancelet and zebrafish RNA-seq data were downloaded from GSE106430/PRJNA416866. Illumina adapter trimming was performed using TrimGalore v0.4.0 (https://github.com/FelixKrueger/TrimGalore). Trimmed sequence reads were aligned to the Spur_v3.1, Bl71nemr and danRer10 reference genomes for sea urchin, lancelet, and zebrafish, respectively, using STAR v2.4.0d. Quantification of transcript abundance was performed using RSEM v1.2.2. TET genes analyzed in this study correspond to the following IDs: WHL22.387614 (SPU_027517) for sea urchin; BL00006 for the European lancelet; and ENSDARG00000075230, ENSDARG00000076928, and ENSDARG00000062646 for zebrafish.

TET protein sequence and structure conservation analysis

Sea urchin TET protein sequence was retrieved from The Universal Protein Resource (UniProt): UniProtKB-A0A7M7NF23 methylcytosine dioxygenase TET (A0A7M7NF23_STRPU). Florida lancelet TET protein sequence was retrieved from the National Center for Biotechnology Information (NCBI): https://ftp.ncbi.nlm.nih.gov/genomes/all/annotation_releases/7739/100/GCF_000003815.2_Bfl_VNyyK/GCF_000003815.2_Bfl_VNyyK_protein.faa.gz, XP_035668917.1 methylcytosine dioxygenase TET1-like isoform X1 (*Branchiostoma floridae*). Fruit fly, zebrafish, mouse, and human TET protein sequences were retrieved from UniProt. To predict TET protein domain structure, amino acid sequences of target sTET, bTET, and zebrafish TET1, TET2, and TET3 proteins in FASTA format were used as input for HMMER (http://hmmer.org/) and SWISS-MODEL. Multiple alignments of TET protein amino acid sequences were performed using UniProt. The Multiple sequence alignment (MSA) comparison was visualized using Jalview 2.11.1.4 (*78*). SWISS-MODEL was used to perform protein structure homology modeling. First, amino acid sequences of target sTET, bTET, and zebrafish TET1, TET2, and TET3 proteins in FASTA format were used as input. 5d9y.1.A (crystal structure of human TET2-5fC complex) and 5exh.1.C (crystal structure of mTET3-CxxC domain in complex with 5caC DNA) were identified as the top-ranked templates based on global model quality estimate, which provides a quality estimate combining the properties from the target-template alignment and the template structure. Sequence identity between the input and 5d9y.1.A template was 57 and 64% for sea urchin sTET and lancelet sTET, respectively; and 71, 75, and 67% for zebrafish TET1, TET2, and TET3, respectively. 5d9y.1.A template was used to build a three-dimensional (3D) model of the TET N-terminal catalytic domain. Model quality was assessed by QMEANDisCo global (the entire structure) quality score, which is a quality measurement ranging between 0 and 1; the closer the score to 1, the higher the expected quality. QMEANDisCo global score was 0.72 and 0.70 for sea urchin sTET and lancelet sTET, respectively; and 0.62, 0.57, and 0.80 for zebrafish TET1, TET2, and TET3, respectively.

Analysis of developmentally hydroxymethylated zebrafish gene orthologs

To assess the temporal and spatial expression of zebrafish orthologs of sea urchin genes linked to 5hmC enrichment (ATAC hmC+ genes), we first identified orthologous genes by converting sea urchin and zebrafish gene IDs to *D. melanogaster* gene IDs using ENSEMBL BioMART tool. Next, sea urchin genes harboring ATAC hmC+ peaks within their promoters or gene bodies were identified. Zebrafish genes, orthologous to sea urchin ATAC hmC+ genes, were used in the downstream analysis. To compare developmental expression dynamics of zebrafish genes having distinct regulatory landscapes after three rounds of whole-genome duplication, we identified zebrafish 2R/3R ohnologs among zebrafish genes, orthologous to the sea urchin ATAC hmC+ genes. 2R and 3R ohnologs [Intermediate: q-score (outgroups) < 0.01 and q-score (self-comparison) < 0.01] were downloaded from http://ohnologs.curie.fr/cgi-bin/BrowsePage.cgi?org=drerio (*62*). Ohnologs were first split into three groups: (i) genes associated with 5hmC-marked ATAC-seq peaks overlapping phylo-DMRs (5hmC/phylo-DMR), (ii) 5hmC-marked ATAC-seq peaks not overlapping phylo-DMRs (5hmC/no phylo-DMR), and (iii) non-5hmC ATAC-seq peaks not overlapping phylo-DMRs (no 5hmC/no phylo-DMR) in their distal regulatory domains. Zebrafish distal regulatory domains were defined using GREAT gene-regulatory domain definition (*54*). Briefly, basal regulatory domains were defined as 5 kb upstream and 1 kb downstream of the TSS, regardless of the neighboring genes. To define distal regulatory domains, basal regulatory domains of each gene were extended upstream and downstream to the neighboring gene's basal domain but no more than 1000 kb in each direction. Twenty-four– and 48-hpf ATAC-seq peaks were downloaded from DANIO-CODE (ATAC-seq_Skarmeta_Lab_0001AS, https://danio-code.zfin.org). Only the ohnologs with at least two different regulatory landscapes (5hmC/phylo-DMR, 5hmC/no phylo-DMR, or no 5hmC/no phylo-DMR) were considered in the downstream bulk RNA-seq and single-cell RNA sequencing (scRNA-seq) analysis.

scRNA-seq data analysis

Zebrafish 24-hpf embryo scRNA-seq InDrop data were downloaded from GSE112294 (*63*). The data were converted to a file format that resembles a 10X Chromium CellRanger output using the indRop R package (https://github.com/caleblareau/indRop) and processed using the standard Seurat pipeline. Briefly, single cells with less than 200 detected genes, more than 4000 detected genes, indicative of

empty droplets and duplicate cells in the droplet, respectively, were discarded. Cells with total Unique molecular identifier (UMI) (transcript) counts less than 1000 and more than 15,000 were excluded from the analysis. Read counts were normalized by a factor of 10,000 and log-transformed. Highly variable features were identified using FindVariableFeatures function. The number of UMIs per cell was regressed out using Seurat's ScaleData function. RunPCA was used to perform linear dimensionality reduction on scaled data using determined highly variable features. Cell clustering was performed using FindNeighbors(object, reduction = "pca", dims = 1:20) and FindClusters(object, resolution = 0.5, algorithm = 1). Nonlinear dimensionality reduction was performed using uniform manifold approximation and projection: RunUMAP(object, reduction = "pca", dims = 1:20).

scRNA-seq downstream analysis

FindAllMarkers function was used to define gene markers for every cluster in the 24-hpf zebrafish embryo. Top 20 genes identified as cluster features (*63*) were matched with the obtained gene markers and used to assign cell clusters to different tissue types. AddModuleScore function was used to define module scores for a set of genes harboring a 5hmC peak and a phylo-DMR (5hmC/phylo-DMR), and genes harboring a 5hmC peak not overlapping a phylo-DMR (5hmC/no phylo-DMR), and genes without a 5hmC peak and without a phylo-DMR (no 5hmC/no phylo-DMR). Positive module score indicates that a given module of genes is more highly expressed in a certain cell than what would be expected from the average expression of this gene module across all cells in the population. Module score was then z-transformed and used in the FeaturePlot. To generate "upset" plots, PrctCellExpringGene function was used to calculate the percentage of cells expressing each of the genes in the 5hmC/phylo-DMR, 5hmC/no phylo-DMR, and no 5hmC/no phylo-DMR gene sets. Genes with nonzero expression counts in more than 25% of cells in any given cluster were deemed expressed in that cluster. UpSetR package upset function was used to display the number of genes in the gene set expressed per cluster, as well as the number of genes expressed across different numbers of clusters.

DNA-sequence motif analysis

Motif analysis of the 5hmC-marked ATAC-seq regions (±250 bp from the ATAC-seq peak summit) associated with promoters or gene bodies was performed using HOMER findMotifsGenome.pl using the default HOMER background normalized for GC content. Motifs were visualized using R package ggseqlogo.

SUPPLEMENTARY MATERIALS

Supplementary material for this article is available at https://science.org/doi/10.1126/sciadv.abn2258

View/request a protocol for this paper from *Bio-protocol*.

REFERENCES AND NOTES

1. E. H. Davidson, J. P. Rast, P. Oliveri, A. Ransick, C. Calestani, C. H. Yuh, T. Minokawa, G. Amore, V. Hinman, C. Arenas-Mena, O. Otim, C. T. Brown, C. B. Livi, P. Y. Lee, R. Revilla, A. G. Rust, Z. Pan, M. J. Schilstra, P. J. Clarke, M. I. Arnone, L. Rowen, R. A. Cameron, D. R. McClay, L. Hood, H. Bolouri, A genomic regulatory network for development. *Science* **295**, 1669–1678 (2002).
2. A. Woolfe, M. Goodson, D. K. Goode, P. Snell, G. K. McEwen, T. Vavouri, S. F. Smith, P. North, H. Callaway, K. Kelly, K. Walter, I. Abnizova, W. Gilks, Y. J. Edwards, J. E. Cooke, G. Elgar, Highly conserved non-coding sequences are associated with vertebrate development. *PLOS Biol.* **3**, e7 (2005).
3. D. Schubeler, Function and information content of DNA methylation. *Nature* **517**, 321–326 (2015).
4. M. V. C. Greenberg, Get out and stay out: New insights into DNA methylation reprogramming in mammals. *Front. Cell Dev. Biol.* **8**, 629068 (2020).
5. N. Rougier, D. Bourc'his, D. M. Gomes, A. Niveleau, M. Plachot, A. Paldi, E. Viegas-Péquignot, Chromosome methylation patterns during mammalian preimplantation development. *Genes Dev.* **12**, 2108–2113 (1998).
6. M. C. Cardoso, H. Leonhardt, DNA methyltransferase is actively retained in the cytoplasm during early development. *J. Cell Biol.* **147**, 25–32 (1999).
7. M. Wossidlo, T. Nakamura, K. Lepikhov, C. J. Marques, V. Zakhartchenko, M. Boiani, J. Arand, T. Nakano, W. Reik, J. Walter, 5-Hydroxymethylcytosine in the mammalian zygote is linked with epigenetic reprogramming. *Nat. Commun.* **2**, 241 (2011).
8. T. P. Gu, F. Guo, H. Yang, H. P. Wu, G. F. Xu, W. Liu, Z. G. Xie, L. Shi, X. He, S. G. Jin, K. Iqbal, Y. G. Shi, Z. Deng, P. E. Szabó, G. P. Pfeifer, J. Li, G. L. Xu, The role of Tet3 DNA dioxygenase in epigenetic reprogramming by oocytes. *Nature* **477**, 606–610 (2011).
9. R. M. Kohli, Y. Zhang, TET enzymes, TDG and the dynamics of DNA demethylation. *Nature* **502**, 472–479 (2013).
10. H. Q. Dai, B. A. Wang, L. Yang, J. J. Chen, G. C. Zhu, M. L. Sun, H. Ge, R. Wang, D. L. Chapman, F. Tang, X. Sun, G. L. Xu, TET-mediated DNA demethylation controls gastrulation by regulating lefty-nodal signalling. *Nature* **538**, 528–532 (2016).
11. O. Bogdanovic, A. H. Smits, E. de la Calle Mustienes, J. J. Tena, E. Ford, R. Williams, U. Senanayake, M. D. Schultz, S. Hontelez, I. van Kruijsbergen, T. Rayon, F. Gnerlich, T. Carell, G. J. Veenstra, M. Manzanares, T. Sauka-Spengler, J. R. Ecker, M. Vermeulen, J. L. Gomez-Skarmeta, R. Lister, Active DNA demethylation at enhancers during the vertebrate phylotypic period. *Nat. Genet.* **48**, 417–426 (2016).
12. S. E. Ross, O. Bogdanovic, Generation and molecular characterization of transient *tet1/2/3* zebrafish knockouts. *Methods Mol. Biol.* **2272**, 281–318 (2021).
13. G. C. Hon, C. X. Song, T. Du, F. Jin, S. Selvaraj, A. Y. Lee, C. A. Yen, Z. Ye, S. Q. Mao, B. A. Wang, S. Kuan, L. E. Edsall, B. S. Zhao, G. L. Xu, C. He, B. Ren, 5mC oxidation by Tet2 modulates enhancer activity and timing of transcriptome reprogramming during differentiation. *Mol. Cell* **56**, 286–297 (2014).
14. C. Li, Y. Lan, L. Schwartz-Orbach, E. Korol, M. Tahiliani, T. Evans, M. G. Goll, Overlapping requirements for Tet2 and Tet3 in normal development and hematopoietic stem cell emergence. *Cell Rep.* **12**, 1133–1143 (2015).
15. K. P. Koh, A. Yabuuchi, S. Rao, Y. Huang, K. Cunniff, J. Nardone, A. Laiho, M. Tahiliani, C. A. Sommer, G. Mostoslavsky, R. Lahesmaa, S. H. Orkin, S. J. Rodig, G. Q. Daley, A. Rao, Tet1 and Tet2 regulate 5-hydroxymethylcytosine production and cell lineage specification in mouse embryonic stem cells. *Cell Stem Cell* **8**, 200–213 (2011).
16. A. Blattler, L. Yao, H. Witt, Y. Guo, C. M. Nicolet, B. P. Berman, P. J. Farnham, Global loss of DNA methylation uncovers intronic enhancers in genes showing expression changes. *Genome Biol.* **15**, 469 (2014).
17. A. de Mendoza, R. Lister, O. Bogdanovic, Evolution of DNA methylome diversity in eukaryotes. *J. Mol. Biol.* **432**, 1687–1705 (2019).
18. P. M. Rae, R. E. Steele, Absence of cytosine methylation at C-C-G-G and G-C-G-C sites in the rDNA coding regions and intervening sequences of *Drosophila* and the rDNA of other insects. *Nucleic Acids Res.* **6**, 2987–2995 (1979).
19. V. J. Simpson, T. E. Johnson, R. F. Hammen, Caenorhabditis elegans DNA does not contain 5-methylcytosine at any time during development or aging. *Nucleic Acids Res.* **14**, 6711–6719 (1986).
20. A. de Mendoza, W. L. Hatleberg, K. Pang, S. Leininger, O. Bogdanovic, J. Pflueger, S. Buckberry, U. Technau, A. Hejnol, M. Adamska, B. M. Degnan, S. M. Degnan, R. Lister, Convergent evolution of a vertebrate-like methylome in a marine sponge. *Nat. Ecol. Evol.* **3**, 1464–1473 (2019).
21. M. M. Suzuki, A. Bird, DNA methylation landscapes: Provocative insights from epigenomics. *Nat. Rev. Genet.* **9**, 465–476 (2008).
22. F. Neri, S. Rapelli, A. Krepelova, D. Incarnato, C. Parlato, G. Basile, M. Maldotti, F. Anselmi, S. Oliviero, Intragenic DNA methylation prevents spurious transcription initiation. *Nature* **543**, 72–77 (2017).
23. T. Dahlet, A. Argüeso Lleida, H. Al Adhami, M. Dumas, A. Bender, R. P. Ngondo, M. Tanguy, J. Vallet, G. Auclair, A. F. Bardet, M. Weber, Genome-wide analysis in the mouse embryo reveals the importance of DNA methylation for transcription integrity. *Nat. Commun.* **11**, 3153 (2020).
24. M. J. Parker, P. R. Weigele, L. Saleh, Insights into the biochemistry, evolution, and biotechnological applications of the ten-eleven translocation (TET) enzymes. *Biochemistry* **58**, 450–467 (2019).
25. B. Delatte, F. Wang, L. V. Ngoc, E. Collignon, E. Bonvin, R. Deplus, E. Calonne, B. Hassabi, P. Putmans, S. Awe, C. Wetzel, J. Kreher, R. Soin, C. Creppe, P. A. Limbach, C. Gueydan, V. Kruys, A. Brehm, S. Minakhina, M. Defrance, R. Steward, F. Fuks, RNA biochemistry. Transcriptome-wide distribution and function of RNA hydroxymethylcytosine. *Science* **351**, 282–285 (2016).
26. M. Wojciechowski, D. Rafalski, R. Kucharski, K. Misztal, J. Maleszka, M. Bochtler, R. Maleszka, Insights into DNA hydroxymethylation in the honeybee from in-depth analyses of TET dioxygenase. *Open Biol.* **4**, 140110 (2014).

27. P. Cingolani, X. Cao, R. S. Khetani, C. C. Chen, M. Coon, A. Sammak, A. Bollig-Fischer, S. Land, Y. Huang, M. E. Hudson, M. D. Garfinkel, S. Zhong, G. E. Robinson, D. M. Ruden, Intronic non-CG DNA hydroxymethylation and alternative mRNA splicing in honey bees. *BMC Genomics* **14**, 666 (2013).
28. L. L. Moroz, K. M. Kocot, M. R. Citarella, S. Dosung, T. P. Norekian, I. S. Povolotskaya, A. P. Grigorenko, C. Dailey, E. Berezikov, K. M. Buckley, A. Ptitsyn, D. Reshetov, K. Mukherjee, T. P. Moroz, Y. Bobkova, F. Yu, V. V. Kapitonov, J. Jurka, Y. V. Bobkov, J. J. Swore, D. O. Girardo, A. Fodor, F. Gusev, R. Sanford, R. Bruders, E. Kittler, C. E. Mills, J. P. Rast, R. Derelle, V. V. Solovyev, F. A. Kondrashov, B. J. Swalla, J. V. Sweedler, E. I. Rogaev, K. M. Halanych, A. B. Kohn, The ctenophore genome and the evolutionary origins of neural systems. *Nature* **510**, 109–114 (2014).
29. F. Marlétaz, P. N. Firbas, I. Maeso, J. J. Tena, O. Bogdanovic, M. Perry, C. D. R. Wyatt, E. de la Calle-Mustienes, S. Bertrand, D. Burguera, R. D. Acemel, S. J. van Heeringen, S. Naranjo, C. Herrera-Ubeda, K. Skvortsova, S. Jimenez-Gancedo, D. Aldea, Y. Marquez, L. Buono, I. Kozmikova, J. Permanyer, A. Louis, B. Albuixech-Crespo, Y. Le Petillon, A. Leon, L. Subirana, P. J. Balwierz, P. E. Duckett, E. Farahani, J. M. Aury, S. Mangenot, P. Wincker, R. Albalat, E. Benito-Gutiérrez, C. Cañestro, F. Castro, S. D'Aniello, D. E. K. Ferrier, S. Huang, V. Laudet, G. A. B. Marais, P. Pontarotti, M. Schubert, H. Seitz, I. Somorjai, T. Takahashi, O. Mirabeau, A. Xu, J. K. Yu, P. Carninci, J. R. Martinez-Morales, H. R. Crollius, Z. Kozmik, M. T. Weirauch, J. Garcia-Fernàndez, R. Lister, B. Lenhard, P. W. H. Holland, H. Escriva, J. L. Gomez-Skarmeta, M. Irimia, Amphioxus functional genomics and the origins of vertebrate gene regulation. *Nature* **564**, 64–70 (2018).
30. Sea Urchin Genome Sequencing Consortium; E. Sodergren, G. M. Weinstock, E. H. Davidson, R. A. Cameron, R. A. Gibbs, R. C. Angerer, L. M. Angerer, M. I. Arnone, D. R. Burgess, R. D. Burke, J. A. Coffman, M. Dean, M. R. Elphick, C. A. Ettensohn, K. R. Foltz, A. Hamdoun, R. O. Hynes, W. H. Klein, W. Marzluff, D. R. McClay, R. L. Morris, A. Mushegian, J. P. Rast, L. C. Smith, M. C. Thorndyke, V. D. Vacquier, G. M. Wessel, G. Wray, L. Zhang, C. G. Elsik, O. Ermolaeva, W. Hlavina, G. Hofmann, P. Kitts, M. J. Landrum, A. J. Mackey, D. Maglott, G. Panopoulou, A. J. Poustka, K. Pruitt, V. Sapojnikov, X. Song, A. Souvorov, V. Solovyev, Z. Wei, C. A. Whittaker, K. Worley, K. J. Durbin, Y. Shen, O. Fedrigo, D. Garfield, R. Haygood, A. Primus, R. Satija, T. Severson, M. L. Gonzalez-Garay, A. R. Jackson, A. Milosavljevic, M. Tong, C. E. Killian, B. T. Livingston, F. H. Wilt, N. Adams, R. Belle, S. Carbonneau, R. Cheung, P. Cormier, B. Cosson, J. Croce, A. Fernandez-Guerra, A. M. Geneviere, M. Goel, H. Kelkar, J. Morales, O. Mulner-Lorillon, A. J. Robertson, J. V. Goldstone, B. Cole, D. Epel, B. Gold, M. E. Hahn, M. Howard-Ashby, M. Scally, J. J. Stegeman, E. L. Allgood, J. Cool, K. M. Judkins, S. S. McCafferty, A. M. Musante, R. A. Obar, A. P. Rawson, B. J. Rossetti, I. R. Gibbons, M. P. Hoffman, A. Leone, S. Istrail, S. C. Materna, M. P. Samanta, V. Stolc, W. Tongprasit, Q. Tu, K. F. Bergeron, B. P. Brandhorst, J. Whittle, K. Berney, D. J. Bottjer, C. Calestani, K. Peterson, E. Chow, Q. A. Yuan, E. Elhaik, D. Graur, J. T. Reese, I. Bosdet, S. Heesun, M. A. Marra, J. Schein, M. K. Anderson, V. Brockton, K. M. Buckley, A. H. Cohen, S. D. Fugmann, T. Hibino, M. Loza-Coll, A. J. Majeske, C. Messier, S. V. Nair, Z. Pancer, D. P. Terwilliger, C. Agca, E. Arboleda, N. Chen, A. M. Churcher, F. Hallbook, G. W. Humphrey, M. M. Idris, T. Kiyama, S. Liang, D. Mellott, X. Mu, G. Murray, R. P. Olinski, F. Raible, M. Rowe, J. S. Taylor, K. Tessmar-Raible, D. Wang, K. H. Wilson, S. Yaguchi, T. Gaasterland, B. E. Galindo, H. J. Gunaratne, C. Juliano, M. Kinukawa, G. W. Moy, A. T. Neill, M. Nomura, M. Raisch, A. Reade, M. M. Roux, J. L. Song, Y. H. Su, I. K. Townley, E. Voronina, J. L. Wong, G. Amore, M. Branno, E. R. Brown, V. Cavalieri, V. Duboc, L. Duloquin, C. Flytzanis, C. Gache, F. Lapraz, T. Lepage, A. Locascio, P. Martinez, G. Matassi, V. Matranga, R. Range, F. Rizzo, E. Rottinger, W. Beane, C. Bradham, C. Byrum, T. Glenn, S. Hussain, G. Manning, E. Miranda, R. Thomason, K. Walton, A. Wikramanayke, S. Y. Wu, R. Xu, C. T. Brown, L. Chen, R. F. Gray, P. Y. Lee, J. Nam, P. Oliveri, J. Smith, D. Muzny, S. Bell, J. Chacko, A. Cree, S. Curry, C. Davis, H. Dinh, S. Dugan-Rocha, J. Fowler, R. Gill, C. Hamilton, J. Hernandez, S. Hines, J. Hume, L. Jackson, A. Jolivet, C. Kovar, S. Lee, L. Lewis, G. Miner, M. Morgan, L. V. Nazareth, G. Okwuonu, D. Parker, L. L. Pu, R. Thorn, R. Wright, The genome of the sea urchin *Strongylocentrotus purpuratus*. *Science* **314**, 941–952 (2006).
31. M. A. Urich, J. R. Nery, R. Lister, R. J. Schmitz, J. R. Ecker, MethylC-seq library preparation for base-resolution whole-genome bisulfite sequencing. *Nat. Protoc.* **10**, 475–483 (2015).
32. E. K. Schutsky, J. E. DeNizio, P. Hu, M. Y. Liu, C. S. Nabel, E. B. Fabyanic, Y. Hwang, F. D. Bushman, H. Wu, R. M. Kohli, Nondestructive, base-resolution sequencing of 5-hydroxymethylcytosine using a DNA deaminase. *Nat. Biotechnol.* **36**, 1083–1090 (2018).
33. N. H. Putnam, T. Butts, D. E. Ferrier, R. F. Furlong, U. Hellsten, T. Kawashima, M. Robinson-Rechavi, E. Shoguchi, A. Terry, J. K. Yu, E. L. Benito-Gutiérrez, I. Dubchak, J. Garcia-Fernàndez, J. J. Gibson-Brown, I. V. Grigoriev, A. C. Horton, P. J. de Jong, J. Jurka, V. V. Kapitonov, Y. Kohara, Y. Kuroki, E. Lindquist, S. Lucas, K. Osoegawa, L. A. Pennacchio, A. A. Salamov, Y. Satou, T. Sauka-Spengler, J. Schmutz, I. T. Shin, A. Toyoda, M. Bronner-Fraser, A. Fujiyama, L. Z. Holland, P. W. Holland, N. Satoh, D. S. Rokhsar, The amphioxus genome and the evolution of the chordate karyotype. *Nature* **453**, 1064–1071 (2008).
34. Y. Xu, C. Xu, A. Kato, W. Tempel, J. G. Abreu, C. Bian, Y. Hu, D. Hu, B. Zhao, T. Cerovina, J. Diao, F. Wu, H. H. He, Q. Cui, E. Clark, C. Ma, A. Barbara, G. J. Veenstra, G. Xu, U. B. Kaiser, X. S. Liu, S. P. Sugrue, X. He, J. Min, Y. Kato, Y. G. Shi, Tet3 CXXC domain and dioxygenase activity cooperatively regulate key genes for *Xenopus* eye and neural development. *Cell* **151**, 1200–1213 (2012).
35. P. Jessop, A. Ruzov, M. Gering, Developmental functions of the dynamic DNA methylome and hydroxymethylome in the mouse and zebrafish: Similarities and differences. *Front. Cell Dev. Biol.* **6**, 27 (2018).
36. P. W. Holland, J. Garcia-Fernàndez, N. A. Williams, A. Sidow, Gene duplications and the origins of vertebrate development. *Dev. Suppl.* **1994**, 125–133 (1994).
37. K. D. Rasmussen, K. Helin, Role of TET enzymes in DNA methylation, development, and cancer. *Genes Dev.* **30**, 733–750 (2016).
38. H. K. Long, N. P. Blackledge, R. J. Klose, ZF-CxxC domain-containing proteins, CpG islands and the chromatin connection. *Biochem. Soc. Trans.* **41**, 727–740 (2013).
39. W. Zhang, W. Xia, Q. Wang, A. J. Towers, J. Chen, R. Gao, Y. Zhang, C. A. Yen, A. Y. Lee, Y. Li, C. Zhou, K. Liu, J. Zhang, T. P. Gu, X. Chen, Z. Chang, D. Leung, S. Gao, Y. H. Jiang, W. Xie, Isoform switch of TET1 regulates DNA demethylation and mouse development. *Mol. Cell* **64**, 1062–1073 (2016).
40. Q. Tu, R. A. Cameron, K. C. Worley, R. A. Gibbs, E. H. Davidson, Gene structure in the sea urchin *Strongylocentrotus purpuratus* based on transcriptome analysis. *Genome Res.* **22**, 2079–2087 (2012).
41. S. Bertrand, J. E. Carvalho, D. Dauga, N. Matentzoglu, V. Daric, J. K. Yu, M. Schubert, H. Escriva, The ontology of the Amphioxus Anatomy and Life Cycle (AMPHX). *Front. Cell Dev. Biol.* **9**, 668025 (2021).
42. J. E. Carvalho, F. Lahaye, L. W. Yong, J. C. Croce, H. Escriva, J. K. Yu, M. Schubert, An updated staging system for cephalochordate development: One table suits them all. *Front. Cell Dev. Biol.* **9**, 668006 (2021).
43. X. Xu, G. Li, C. Li, J. Zhang, Q. Wang, D. K. Simmons, X. Chen, N. Wijesena, W. Zhu, Z. Wang, Z. Wang, B. Ju, W. Ci, X. Lu, D. Yu, Q. F. Wang, N. Aluru, P. Oliveri, Y. E. Zhang, M. Q. Martindale, J. Liu, Evolutionary transition between invertebrates and vertebrates via methylation reprogramming in embryogenesis. *Natl. Sci. Rev.* **6**, 993–1003 (2019).
44. G. C. Hon, N. Rajagopal, Y. Shen, D. F. McCleary, F. Yue, M. D. Dang, B. Ren, Epigenetic memory at embryonic enhancers identified in DNA methylation maps from adult mouse tissues. *Nat. Genet.* **45**, 1198–1206 (2013).
45. R. Albalat, J. Martí-Solans, C. Cañestro, DNA methylation in amphioxus: From ancestral functions to new roles in vertebrates. *Brief. Funct. Genomics* **11**, 142–155 (2012).
46. A. de Mendoza, D. Poppe, S. Buckberry, J. Pflueger, C. B. Albertin, T. Daish, S. Bertrand, E. de la Calle-Mustienes, J. L. Gómez-Skarmeta, J. R. Nery, J. R. Ecker, B. Baer, C. W. Ragsdale, F. Grutzner, H. Escriva, B. Venkatesh, O. Bogdanovic, R. Lister, The emergence of the brain non-CpG methylation system in vertebrates. *Nat. Ecol. Evol.* **5**, 369–378 (2021).
47. J. Liu, H. Hu, S. Panserat, L. Marandel, Evolutionary history of DNA methylation related genes in chordates: New insights from multiple whole genome duplications. *Sci. Rep.* **10**, 970 (2020).
48. M. Pradhan, P. O. Esteve, H. G. Chin, M. Samaranayke, G. D. Kim, S. Pradhan, CXXC domain of human DNMT1 is essential for enzymatic activity. *Biochemistry* **47**, 10000–10009 (2008).
49. F. Aniello, A. Locascio, L. Fucci, G. Geraci, M. Branno, Isolation of cDNA clones encoding DNA methyltransferase of sea urchin P. lividus: Expression during embryonic development. *Gene* **178**, 57–61 (1996).
50. M. Yu, G. C. Hon, K. E. Szulwach, C. X. Song, L. Zhang, A. Kim, X. Li, Q. Dai, Y. Shen, B. Park, J. H. Min, P. Jin, B. Ren, C. He, Base-resolution analysis of 5-hydroxymethylcytosine in the mammalian genome. *Cell* **149**, 1368–1380 (2012).
51. K. Skvortsova, E. Zotenko, P. L. Luu, C. M. Gould, S. S. Nair, S. J. Clark, C. Stirzaker, Comprehensive evaluation of genome-wide 5-hydroxymethylcytosine profiling approaches in human DNA. *Epigenetics Chromatin* **10**, 16 (2017).
52. K. Skvortsova, O. Bogdanovic, TAB-seq and ACE-seq data processing for genome-Wide DNA hydroxymethylation profiling. *Methods Mol. Biol.* **2272**, 163–178 (2021).
53. J. Reimand, M. Kull, H. Peterson, J. Hansen, J. Vilo, g:Profiler—A web-based toolset for functional profiling of gene lists from large-scale experiments. *Nucleic Acids Res.* **35**, W193–W200 (2007).
54. C. Y. McLean, D. Bristor, M. Hiller, S. L. Clarke, B. T. Schaar, C. B. Lowe, A. M. Wenger, G. Bejerano, GREAT improves functional interpretation of cis-regulatory regions. *Nat. Biotechnol.* **28**, 495–501 (2010).
55. J. Zeitlinger, A. Stark, Developmental gene regulation in the era of genomics. *Dev. Biol.* **339**, 230–239 (2010).
56. L. Vanzan, H. Soldati, V. Ythier, S. Anand, S. M. G. Braun, N. Francis, R. Murr, High throughput screening identifies SOX2 as a super pioneer factor that inhibits DNA methylation maintenance at its binding sites. *Nat. Commun.* **12**, 3337 (2021).
57. Y. A. Yang, J. C. Zhao, K. W. Fong, J. Kim, S. Li, C. Song, B. Song, B. Zheng, C. He, J. Yu, FOXA1 potentiates lineage-specific enhancer activation through modulating TET1 expression and function. *Nucleic Acids Res.* **44**, 8153–8164 (2016).
58. G. Ficz, M. R. Branco, S. Seisenberger, F. Santos, F. Krueger, T. A. Hore, C. J. Marques, S. Andrews, W. Reik, Dynamic regulation of 5-hydroxymethylcytosine in mouse ES cells and during differentiation. *Nature* **473**, 398–402 (2011).

59. Y. Li, H. Zheng, Q. Wang, C. Zhou, L. Wei, X. Liu, W. Zhang, Y. Zhang, Z. Du, X. Wang, W. Xie, Genome-wide analyses reveal a role of Polycomb in promoting hypomethylation of DNA methylation valleys. *Genome Biol.* **19**, 18 (2018).
60. X. Wu, H. Zhang, B. Zhang, Y. Zhang, Q. Wang, W. Shen, X. Wu, L. Li, W. Xia, R. Nakamura, B. Liu, F. Liu, H. Takeda, A. Meng, W. Xie, Methylome inheritance and enhancer dememorization reset an epigenetic gate safeguarding embryonic programs. *Sci. Adv.* **7**, eabl3858 (2021).
61. P. Dehal, J. L. Boore, Two rounds of whole genome duplication in the ancestral vertebrate. *PLoS Biol.* **3**, e314 (2005).
62. P. P. Singh, H. Isambert, OHNOLOGS v2: A comprehensive resource for the genes retained from whole genome duplication in vertebrates. *Nucleic Acids Res.* **48**, D724–D730 (2020).
63. D. E. Wagner, C. Weinreb, Z. M. Collins, J. A. Briggs, S. G. Megason, A. M. Klein, Single-cell mapping of gene expression landscapes and lineage in the zebrafish embryo. *Science* **360**, 981–987 (2018).
64. H. Yang, Y. Luan, T. Liu, H. J. Lee, L. Fang, Y. Wang, X. Wang, B. Zhang, Q. Jin, K. C. Ang, X. Xing, J. Wang, J. Xu, F. Song, I. Sriranga, C. Khunsriraksakul, T. Salameh, D. Li, M. N. K. Choudhary, J. Topczewski, K. Wang, G. S. Gerhard, R. C. Hardison, T. Wang, K. C. Cheng, F. Yue, A map of cis-regulatory elements and 3D genome structures in zebrafish. *Nature* **588**, 337–343 (2020).
65. A. M. Deaton, A. Bird, CpG islands and the regulation of transcription. *Genes Dev.* **25**, 1010–1022 (2011).
66. T. A. Hore, F. von Meyenn, M. Ravichandran, M. Bachman, G. Ficz, D. Oxley, F. Santos, S. Balasubramanian, T. P. Jurkowski, W. Reik, Retinol and ascorbate drive erasure of epigenetic memory and enhance reprogramming to naïve pluripotency by complementary mechanisms. *Proc. Natl. Acad. Sci. U.S.A.* **113**, 12202–12207 (2016).
67. W. A. Pastor, L. Aravind, A. Rao, TETonic shift: Biological roles of TET proteins in DNA demethylation and transcription. *Nat. Rev. Mol. Cell Biol.* **14**, 341–356 (2013).
68. S. Domcke, A. F. Bardet, P. Adrian Ginno, D. Hartl, L. Burger, D. Schubeler, Competition between DNA methylation and transcription factors determines binding of NRF1. *Nature* **528**, 575–579 (2015).
69. C. W. Lio, J. Zhang, E. Gonzalez-Avalos, P. G. Hogan, X. Chang, A. Rao, Tet2 and Tet3 cooperate with B-lineage transcription factors to regulate DNA modification and chromatin accessibility. *eLife* **5**, e18290 (2016).
70. M. Jinek, K. Chylinski, I. Fonfara, M. Hauer, J. A. Doudna, E. Charpentier, A programmable dual-RNA-guided DNA endonuclease in adaptive bacterial immunity. *Science* **337**, 816–821 (2012).
71. G. Kushawah, L. Hernandez-Huertas, J. Abugattas-Nuñez Del Prado, J. R. Martinez-Morales, M. L. DeVore, H. Hassan, I. Moreno-Sanchez, L. Tomas-Gallardo, A. Diaz-Moscoso, D. E. Monges, J. R. Guelfo, W. C. Theune, E. O. Brannan, W. Wang, T. J. Corbin, A. M. Moran, A. Sánchez Alvarado, E. Malaga-Trillo, C. M. Takacs, A. A. Bazzini, M. A. Moreno-Mateos, CRISPR-Cas13d induces efficient mRNA knockdown in animal embryos. *Dev. Cell* **54**, 805–817.e7 (2020).
72. M. Levin, L. Anavy, A. G. Cole, E. Winter, N. Mostov, S. Khair, N. Senderovich, E. Kovalev, D. H. Silver, M. Feder, S. L. Fernandez-Valverde, N. Nakanishi, D. Simmons, O. Simakov, T. Larsson, S. Y. Liu, A. Jerafi-Vider, K. Yaniv, J. F. Ryan, M. Q. Martindale, J. C. Rink, D. Arendt, S. M. Degnan, B. M. Degnan, T. Hashimshony, I. Yanai, The mid-developmental transition and the evolution of animal body plans. *Nature* **531**, 637–641 (2016).
73. M. Fuentes, E. Benito, S. Bertrand, M. Paris, A. Mignardot, L. Godoy, S. Jimenez-Delgado, D. Oliveri, S. Candiani, E. Hirsinger, S. D'Aniello, J. Pascual-Anaya, I. Maeso, M. Pestarino, P. Vernier, J. F. Nicolas, M. Schubert, V. Laudet, A. M. Geneviere, R. Albalat, J. Garcia Fernandez, N. D. Holland, H. Escriva, Insights into spawning behavior and development of the European amphioxus (Branchiostoma lanceolatum). *J. Exp. Zool. B Mol. Dev. Evol.* **308**, 484–493 (2007).
74. M. S. Magri, D. Voronov, J. Ranđelović, C. Cuomo, J. L. Gómez-Skarmeta, M. I. Arnone, ATAC-seq for assaying chromatin accessibility protocol using echinoderm embryos. *Methods Mol. Biol.* **2219**, 253–265 (2021).
75. H. Li, B. Handsaker, A. Wysoker, T. Fennell, J. Ruan, N. Homer, G. Marth, G. Abecasis, R. Durbin; 1000 Genome Project Data Processing Subgroup, The sequence alignment/map format and SAMtools. *Bioinformatics* **25**, 2078–2079 (2009).
76. B. Langmead, S. L. Salzberg, Fast gapped-read alignment with Bowtie 2. *Nat. Methods* **9**, 357–359 (2012).
77. Y. Zhang, T. Liu, C. A. Meyer, J. Eeckhoute, D. S. Johnson, B. E. Bernstein, C. Nusbaum, R. M. Myers, M. Brown, W. Li, X. S. Liu, Model-based analysis of ChIP-Seq (MACS). *Genome Biol.* **9**, R137 (2008).
78. A. M. Waterhouse, J. B. Procter, D. M. Martin, M. Clamp, G. J. Barton, Jalview version 2—A multiple sequence alignment editor and analysis workbench. *Bioinformatics* **25**, 1189–1191 (2009).

Acknowledgments: We thank A. de Mendoza for critical reading of the manuscript, P. Leahy for providing adult sea urchins, and D. Caramiello for sea urchin care. Drawings of adult sea urchin, lancelet, and zebrafish were created with BioRender.com. **Funding:** The Australian Research Council (ARC) Discovery Project (DP190103852), Ramón y Cajal fellowship from the Spanish Ministry of Science and Innovation (RYC2020-028685-I), and funding from CEX2020-00108-M Unidad de Excelencia María de Maeztu to O.B. supported this work. **Author contributions:** O.B. and K.S. designed the study. M.I.A., H.E., and J.L.G.S. contributed to concept and study design. Sea urchin embryo and adult tissue collection and DNA extraction were performed by D.V. and M.I.A. Lancelet embryo and adult tissue collection and DNA extraction were performed by S.B. and H.E. MethylC-seq library preparation and sequencing were carried out by P.E.D. and S.E.R. ACE-seq library preparation and sequencing were carried out by K.S. Sea urchin ATAC-seq library preparation was carried out by M.S.M., D.V., M.I.A., and I.M., and sequencing was carried out by M.S.M. and I.M. K.S. performed data analysis. O.B. and R.J.W. participated in data analysis. K.S. and O.B. wrote the manuscript. All authors discussed the results and commented on the manuscript. **Competing interests:** The authors declare that they have no competing interests. **Data and materials availability:** MethylC-Seq, ACE-seq, and ATAC-seq data generated in this study are available from NCBI Gene Expression Omnibus (GEO SuperSeries accession number GSE188334). Specifically, sea urchin and lancelet MethylC-seq is available under GSE188333. Sea urchin, lancelet, and zebrafish ACE-seq data are available under GSE188331. Sea urchin, lancelet, and zebrafish hMeDIP-seq data are available under GSE188332. Sea urchin ATAC-seq data are available under GSE186363. Public lancelet and zebrafish ATAC-seq data are available under GSE106428. Public sea urchin RNA-seq data are available under PRJNA81157. Public lancelet and zebrafish RNA-seq data are available under GSE106430/PRJNA416866. Public scRNA-seq data of zebrafish 24-hpf embryo are available under GSE112294. All data needed to evaluate the conclusions in the paper are present in the paper and/or the Supplementary Materials.

Submitted 12 November 2021
Accepted 19 October 2022
Published 2 December 2022
10.1126/sciadv.abn2258

ScienceAdvances

Active DNA demethylation of developmental *cis*-regulatory regions predates vertebrate origins

Ksenia SkvortsovaStephanie BertrandDanila VoronovPaul E. DuckettSamuel E. RossMarta Silvia MagriIgnacio MaesoRobert J. WeatheritJose Luis Gómez SkarmetaMaria Ina ArnoneHector EscrivaOzren Bogdanovic

Sci. Adv., 8 (48), eabn2258. • DOI: 10.1126/sciadv.abn2258

Science Advances (ISSN) is published by the American Association for the Advancement of Science. 1200 New York Avenue NW, Washington, DC 20005. The title *Science Advances* is a registered trademark of AAAS.